JOC The Journal of Organic Chemistry

Article

pubs.acs.org/joc

Transannular E···E′ Interactions in Neutral, Radical Cationic, and Dicationic Forms of *cyclo*-[E($CH_2CH_2CH_2$)$_2$E′] (E, E′ = S, Se, Te, and O) with Structural Feature: Dynamic and Static Behavior of E···E′ Elucidated by QTAIM Dual Functional Analysis

Satoko Hayashi,* Kohei Matsuiwa, Nozomu Nishizawa, and Waro Nakanishi*

Department of Material Science and Chemistry, Faculty of Systems Engineering, Wakayama University, 930 Sakaedani, Wakayama 640-8510, Japan

Supporting Information

ABSTRACT: The nature of the transannular E-∗-E′ interactions in neutral, radical cationic, and dicationic forms of *cyclo*-E($CH_2CH_2CH_2$)$_2$E′ (**1**) (E, E′ = S, Se, Te, and O) (**1**, $\mathbf{1}^{\bullet+}$, and $\mathbf{1}^{2+}$, respectively) is elucidated by applying QTAIM dual functional analysis (QTAIM-DFA). $H_b(\mathbf{r}_c)$ are plotted versus $H_b(\mathbf{r}_c) - V_b(\mathbf{r}_c)/2$ for the data of E-∗-E′ at BCPs in QTAIM-DFA, where ∗ emphasizes the existence of BCP. Plots for the fully optimized structures are analyzed by the polar coordinate (R, θ) representation. Those containing the perturbed structures are by (θ_p, κ_p): θ_p corresponds to the tangent line of the plot, and κ_p is the curvature. While (R, θ) describes the static nature, (θ_p, κ_p) represents the dynamic nature of interactions. The nature is well-specified by (R, θ) and (θ_p, κ_p). E-∗-E′ becomes stronger in the order of $\mathbf{1} < \mathbf{1}^{\bullet+} < \mathbf{1}^{2+}$, except for O-∗-O. While E-∗-E′ (E, E′ = S, Se, and Te) in $\mathbf{1}^{2+}$ are characterized as weak covalent bonds, except for S-∗-Te (MC nature through CT) and Se-∗-Te (TBP nature through CT), O-∗-E′ seems more complex. The behavior of E-∗-E′ in $\mathbf{1}^{2+}$ is very close to that of *cyclo*-E($CH_2CH_2CH_2$)E′ (E, E′ = S, Se, Te, and O), except for O-∗-O.

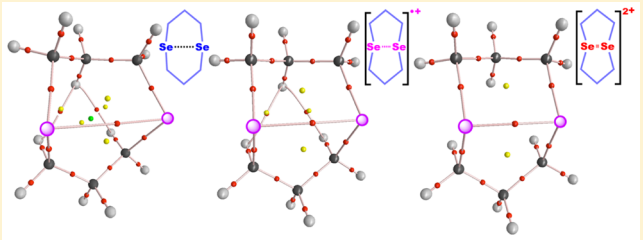

INTRODUCTION

Chalcogen−chalcogen interactions (E−E′ and E···E′: E, E′ = S, Se, and Te, together with O) are of current and continuous interest, not only those of the shared-shell (SS) type (E−E′) but also of the closed-shell (CS) type (E···E′).[1−6] The E−E′ bonds play an important role in all fields of chemical and biological sciences. They maintain peptide structures and biological activities in enzymes, especially for E, E′ = S, Se.[7−11] The E−E′ bonds in dichalcogenides (RE−E′R′) supply low-lying vacant orbitals of the σ-type (σ∗(E−E′)), where the E/E′ atoms contain lone pair orbitals of s- and p-types (n_s(E/E′) and n_p(E/E′), respectively) of relatively high energy levels. Consequently, the E−E′ bonds in RE−E′R′ are easily oxidized and reduced, which is important to develop highly functionalized materials. On the other hand, the intermolecular E···E′ interactions of the CS type are often encountered in crystals of organic compounds containing chalcogen atoms, which must be the important driving force to grow the crystals, and they create useful properties of materials. 1,8-(Dichalcogena)naphthalenes and the related species must be the typical systems for the intramolecular E···E′ interactions.[12]

1,5-(Dichalcogena)canes and the related species also supply a typical system to study the E···E′ interactions. Research groups of Furukawa[13−22] and Glass[23−27] have investigated the transannular E···E′ interactions in *cyclo*-E($CH_2CH_2CH_2$)$_2$E′ (**1**) with some (E, E′) of (S, S: **a**), (S, Se: **b**), (S, Te: **c**), (Se, Se: **d**), (Se, Te: **e**), (Te, Te: **f**), (O, O: **g**), (O, S: **h**), (O, Se: **i**), and (O, Te: **j**) (Chart 1). E and E′ are chosen so that the electronegativity of E (χ_E) is larger than or equal to that of E′ ($\chi_{E'}$) ($\chi_E \geq \chi_{E'}$).[28] The transannular E···E′ interactions at the 1,5-positions of the eight-membered ring in **1** are expected to be highly advantageous due to the formation of two fused five-membered rings. One-electron oxidation of 1,5-dithiocane (**1a**) will give a radical cation $\mathbf{1a}^{\bullet+}$, which can be described as a rather stable species. Its EPR spectrum persists for at least 72 h at

Chart 1. 1,5-(Dichalcogena)canes and the Related Species

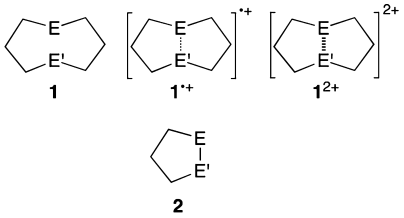

(E, E′) = **a**: (S, S), **b**: (S, Se), **c**: (S, Te)
d: (Se, Se), **e**: (Se, Te), **f**: (Te, Te)
g: (O, O), **h**: (O, S), **i**: (O, Se), **j**: (O, Te)

Received: August 3, 2015
Published: November 10, 2015

DOI: 10.1021/acs.joc.5b01794
J. Org. Chem. 2015, 80, 11963−11976

room temperature.[29] Two fused five-membered rings through the transannular S−S interaction in $\mathbf{1a}^{\bullet+}$ must be responsible for the remarkable stability of $\mathbf{1a}^{\bullet+}$.[29,30] Three energetically favored *cis*-fused conformers are predicted through the conformational analysis, which are chair−boat (**CB**), chair−chair (**CC**), and boat−boat (**BB**) conformers. The **CB** conformer is shown to be the global minimum, which is more stable than **CC** and **BB** by about 8 kJ mol^{-1}.[27,31] $\mathbf{1a}^{\bullet+}$ is further oxidized to give a dication $\mathbf{1a}^{2+}$, and the structure is determined by X-ray crystallographic analysis.[13] The transannular interactions are also investigated for **1b**−**1f**. Among the species, the structure of $\mathbf{1d}^{2+}$ is reported,[14] together with those of $[\mathbf{1b}-\mathbf{1b}]^{2+}$ and $\mathbf{1c}^{2+}$.[26] Dimer dications could be produced in the dimerization of the corresponding monomer radical cations or the reaction of the monomer dications with the corresponding neutral monomers.

Figure 1 shows the structures of $\mathbf{1a}^{2+}$, $\mathbf{1c}^{2+}$, and $\mathbf{1d}^{2+}$, determined by X-ray analysis,[13,14] where the counteranions are

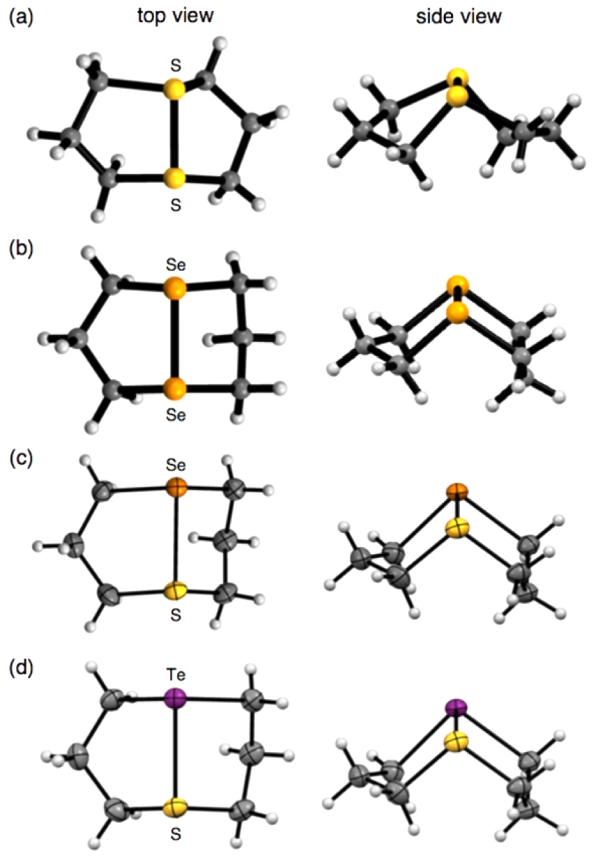

Figure 1. Observed structures of $\mathbf{1a}^{2+}$ (**CC**: KAGHOP)[13] (a) and $\mathbf{1d}^{2+}$ (**CB**: KIVHIG)[14] (b), together with $\mathbf{1b}^{\bullet+}$ (**CB**) (half structure of $[\mathbf{1b}-\mathbf{1b}]^{2+}$: GUYRUO)[26] (c) and $\mathbf{1c}^{2+}$ (**CB**: GUYSID)[26] (d).

neglected. Figure 2 draws the structures of $\mathbf{1a}^{\bullet+}$ (**CB**), $\mathbf{1a}^{\bullet+}$ (**CC**), and $\mathbf{1a}^{\bullet+}$ (**BB**), optimized at the MP2 level as a beginning of this work. $\mathbf{1a}^{\bullet+}$ (**CB**) is shown to have C_s symmetry and to be more stable than $\mathbf{1a}^{\bullet+}$ (**CC**) and $\mathbf{1a}^{\bullet+}$ (**BB**) by 12.0 and 10.1 kJ mol^{-1}, respectively, under the calculation conditions employed in this work. The optimized structure of $\mathbf{1a}^{\bullet+}$ (**BB**) has C_2 symmetry, which is somewhat twisted from the C_{2v} symmetry. That of $\mathbf{1a}^{\bullet+}$ (**CC**) also has the C_2 symmetry. The results of the calculations on $\mathbf{1a}^{\bullet+}$ supported the previous observations. While the observed structure of $\mathbf{1a}^{2+}$

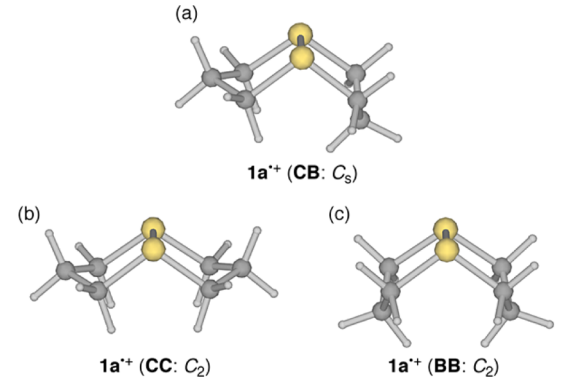

Figure 2. Optimized structures of $\mathbf{1a}^{\bullet+}$ (**CB**: C_s) (a), $\mathbf{1a}^{\bullet+}$ (**CC**: C_2) (b), and $\mathbf{1a}^{\bullet+}$ (**BB**: C_2) (c).

is the **CC** type with substantial deformation (twisted: KAGHOP),[13] those of $\mathbf{1d}^{2+}$ (KIVHIG) and $\mathbf{1c}^{2+}$ (**CB**) (GUYSID)[26] are the **CB** type without substantial deformation.[14] The structure of $\mathbf{1b}^{\bullet+}$ (GUYRUO)[26] is also the **CB** type as shown in Figure 1, although the half structure of $[\mathbf{1b}-\mathbf{1b}]^{2+}$ is drawn for $\mathbf{1b}^{\bullet+}$. Substantial deformations are not found in the components, although the environmental conditions must be different for the head and tail positions in the components when dimers are formed from the corresponding monomers. As a result, the **CB** type must be most important for the structures of $\mathbf{1}^{\bullet+}$ and $\mathbf{1}^{2+}$. The **CC** structure should also be taken into account in some cases, since the structure of $\mathbf{1a}^{2+}$ is observed as **CC**. Figure 3 illustrates MO descriptions for the chalcogen−chalcogen interactions in **1**, $\mathbf{1}^{\bullet+}$, and $\mathbf{1}^{2+}$, which are to be clarified in this work.

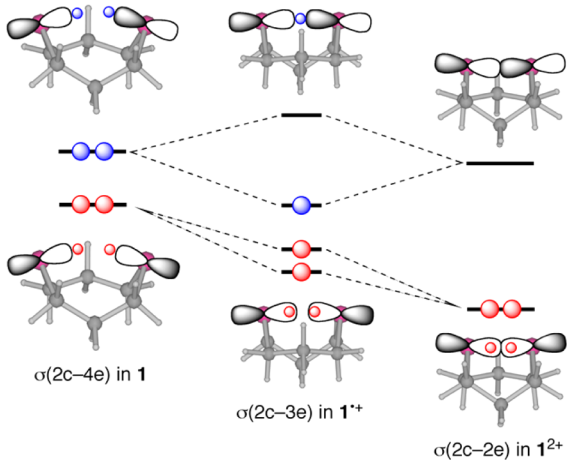

Figure 3. MO descriptions for the chalcogen−chalcogen interactions in **1**, $\mathbf{1}^{\bullet+}$, and $\mathbf{1}^{2+}$ of the **CB** type (cf., Figure 8).

QTAIM (the quantum theory of atoms-in-molecules) approach, introduced by Bader,[32,33] enables us to analyze the nature of chemical bonds and interactions.[34−38] Lots of QTAIM investigations have been reported so far;[39−46] however, there are not many from the viewpoint of experimental chemists. We searched for such methods that enable experimental chemists to analyze their own results, concerning chemical bonds and interactions, by their own image and recently proposed QTAIM dual functional analysis (QTAIM-DFA).[47−49] QTAIM-DFA will provide an excellent

DOI: 10.1021/acs.joc.5b01794
J. Org. Chem. 2015, 80, 11963−11976

possibility to evaluate, understand, and classify weak to strong interactions in a unified form.

We consider QTAIM-DFA to be well-suited to clarify the dynamic and static behavior of the E−E′ and E···E′ interactions (E, E′ = S, Se, Te, and O). The structures of $\mathbf{1}^{\bullet+}$ and $\mathbf{1}^{2+}$ are investigated, and some pictures for the E···E′ interactions are proposed, so far. However, the nature of the E···E′ interactions must be clarified further for better understanding of the phenomena derived from the interactions, with phsycal necessity. Here we report the behavior of the E···E′ interactions in $\mathbf{1}^{\bullet+}$ and $\mathbf{1}^{2+}$, together with **1**, by applying QTAIM-DFA. The behavior of E···E′ in $\mathbf{1}^{\bullet+}$ and $\mathbf{1}^{2+}$ must be closely related to that of E−E′ in the neutral and ionic forms of *cyclo*-1,2-EE′$(CH_2)_3$ (**2**: E, E′ = S, Se, Te, and O), together with HEE′H and MeEE′Me, reported recently by applying QTAIM-DFA.[50]

QTAIM-DFA is surveyed next, together with some basic concept of the QTAIM approach.

QTAIM-DFA (QTAIM Dual Functional Analysis). The bond critical point (BCP; ∗) is an important concept in QTAIM. BCP of $(\omega, \sigma) = (3, -1)$[32] is a point along the bond path (BP) at the interatomic surface, where $\rho(\mathbf{r})$ reaches a minimum. It is denoted by $\rho_b(\mathbf{r}_c)$. While the chemical bonds or interactions between A and B are denoted by A−B, in general, which correspond to BPs between A and B in QTAIM, A-∗-B emphasizes the presence of BCP (∗) in A−B.

While $\rho_b(\mathbf{r}_c)$ is locally depleted relative to the average distribution around the critical points $\mathbf{r}_c$ if $\nabla^2\rho_b(\mathbf{r}_c) > 0$, it is concentrated when $\nabla^2\rho_b(\mathbf{r}_c) < 0$. Total electron energy densities at BCPs ($H_b(\mathbf{r}_c)$) must be a more appropriate measure for weak interactions on the energy basis.[32,33,46−49] $H_b(\mathbf{r}_c)$ expressions are the sum of kinetic energy densities ($G_b(\mathbf{r}_c)$) and potential energy densities ($V_b(\mathbf{r}_c)$) at BCPs, as shown in eq 1. Electrons at BCPs are stabilized when $H_b(\mathbf{r}_c) < 0$; therefore, interactions exhibit covalent nature in this region, whereas they exhibit no covalency if $H_b(\mathbf{r}_c) > 0$, due to the destabilization of electrons at BCPs under the conditions.[32] Equation 2 represents the relation between $\nabla^2\rho_b(\mathbf{r}_c)$ and $H_b(\mathbf{r}_c)$, together with $G_b(\mathbf{r}_c)$ and $V_b(\mathbf{r}_c)$, which is closely related to the virial theorem.

$$H_b(\mathbf{r}_c) = G_b(\mathbf{r}_c) + V_b(\mathbf{r}_c) \quad (1)$$

$$(\hbar^2/8m)\nabla^2\rho_b(\mathbf{r}_c) = H_b(\mathbf{r}_c) - V_b(\mathbf{r}_c)/2 = G_b(\mathbf{r}_c) + V_b(\mathbf{r}_c)/2 \quad (2)$$

Interactions are classified by the signs of $\nabla^2\rho_b(\mathbf{r}_c)$ and $H_b(\mathbf{r}_c)$. Interactions in the region of $\nabla^2\rho_b(\mathbf{r}_c) < 0$ are called shared-shell (SS) interactions,[32a] and they are closed-shell (CS) interactions for $\nabla^2\rho_b(\mathbf{r}_c) > 0$. $H_b(\mathbf{r}_c)$ must be negative when $\nabla^2\rho_b(\mathbf{r}_c) < 0$ (eq 2); therefore, $\nabla^2\rho_b(\mathbf{r}_c) < 0$ and $H_b(\mathbf{r}_c) < 0$ for the SS interactions. The CS interactions are especially called pure CS interactions for $H_b(\mathbf{r}_c) > 0$ and $\nabla^2\rho_b(\mathbf{r}_c) > 0$.[32a] Electrons in the intermediate region between SS and pure CS are locally depleted but stabilized at BCPs.[32a] We call the interactions in this region regular CS,[47,48] when it is necessary to distinguish this from pure CS. The role of $\nabla^2\rho_b(\mathbf{r}_c)$ in the classification can be replaced by $H_b(\mathbf{r}_c) - V_b(\mathbf{r}_c)/2$, since $(\hbar^2/8m)\nabla^2\rho_b(\mathbf{r}_c) = H_b(\mathbf{r}_c) - V_b(\mathbf{r}_c)/2$ (eq 2).

We proposed QTAIM-DFA by plotting $H_b(\mathbf{r}_c)$ versus $H_b(\mathbf{r}_c) - V_b(\mathbf{r}_c)/2$ $(=(\hbar^2/8m)\nabla^2\rho_b(\mathbf{r}_c))$,[47a] after the proposal of $H_b(\mathbf{r}_c)$ versus $\nabla^2\rho_b(\mathbf{r}_c)$.[47b] Both axes in the plot of the former are given in energy units; therefore, distances on the (x, y) $(=(H_b(\mathbf{r}_c) - V_b(\mathbf{r}_c)/2, H_b(\mathbf{r}_c))$ plane can be expressed in the energy unit. QTAIM-DFA can incorporate the classification of interactions by the signs of $\nabla^2\rho_b(\mathbf{r}_c)$ and $H_b(\mathbf{r}_c)$. Scheme 1 summarizes the

Scheme 1. QTAIM-DFA: Plot of $H_b(r_c)$ versus $H_b(r_c) - V_b(r_c)/2$ for Weak to Strong Interactions

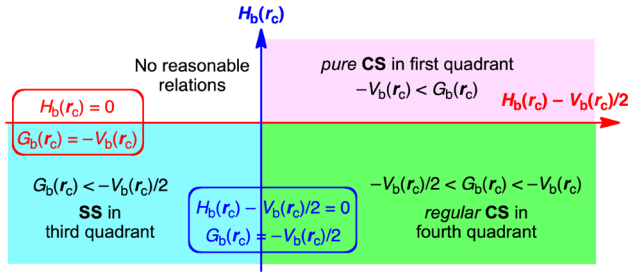

QTAIM-DFA treatment. Interactions of pure CS appear in the first quadrant, those of regular CS in the fourth quadrant, and SS in the third one. No interactions appear in the second.

In our treatment, data for perturbed structures around fully optimized ones are employed for the plots, in addition to those of the fully optimized structures (see Figure 4).[47−49] Plots of

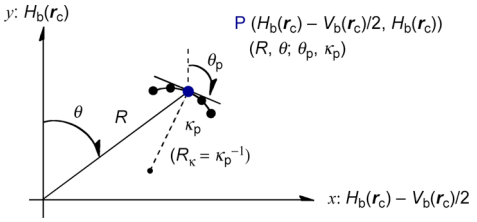

Figure 4. Polar coordinate (R, θ) representation of $H_b(\mathbf{r}_c)$ versus $H_b(\mathbf{r}_c) - V_b(\mathbf{r}_c)/2$, with (θ_p, κ_p) parameters.

$H_b(\mathbf{r}_c)$ versus $H_b(\mathbf{r}_c) - V_b(\mathbf{r}_c)/2$ are analyzed employing the polar coordinate (R, θ) representation with the (θ_p, κ_p) parameters.[47a,48,49] Figure 4 explains the treatment. R in (R, θ) corresponds to the energy for an interaction at BCP, which is defined by eq 3. θ in (R, θ) controls the spiral stream observed in the plot, as defined by eq 4 and measured from the y-axis. Each plot for an interaction shows a specific curve, which provides important information on the interaction (see Figure 4). The curve is expressed by (θ_p, κ_p). While θ_p corresponds to the tangent line of a plot, measured from the y-direction (eq 5), κ_p is the curvature (eq 6). We proposed the concept of the "dynamic nature of interaction" that originated from data of the perturbed structures. While (R, θ) for the data of fully optimized structures correspond to the static nature, (θ_p, κ_p) for those containing the perturbed structures represent the dynamic nature of interactions. The method to generate the perturbed structures is discussed later. While $\rho_b(\mathbf{r}_c)$, $\nabla^2\rho_b(\mathbf{r}_c)$, $G_b(\mathbf{r}_c)$, $V_b(\mathbf{r}_c)$, $H_b(\mathbf{r}_c)$, $H_b(\mathbf{r}_c) - V_b(\mathbf{r}_c)/2$, and $k_b(\mathbf{r}_c)$, defined by eq 7, belong to QTAIM functions, (R, θ) and (θ_p, κ_p) are called QTAIM-DFA parameters. $k_b(\mathbf{r}_c)$ will be treated as if it was an QTAIM parameter, if suitable.

$$R = (x^2 + y^2)^{1/2} \quad (3)$$

$$\theta = 90° - \tan^{-1}(y/x) \quad (4)$$

$$\theta_p = 90° - \tan^{-1}(dy/dx) \quad (5)$$

$$\kappa_p = |d^2y/dx^2|/[1 + (dy/dx)^2]^{3/2} \quad (6)$$

DOI: 10.1021/acs.joc.5b01794
J. Org. Chem. 2015, 80, 11963−11976

$$k_b(\mathbf{r}_c) = V_b(\mathbf{r}_c)/G_b(\mathbf{r}_c) \quad (7)$$

where

$$(x, y) = (H_b(\mathbf{r}_c) - V_b(\mathbf{r}_c)/2, H_b(\mathbf{r}_c))$$

Criteria for Classification and Characterization of Interactions: Application of QTAIM-DFA to Typical Interactions. QTAIM-DFA is applied to typical interactions of van der Waals interactions (vdW), hydrogen bonds (HBs), molecular complexes formed through CT (CT-MC), trihalide ions (X_3^-), trigonal bipyramidal adducts formed through CT (CT-TBP), weak covalent bonds (Cov-w), and strong covalent bonds (Cov-s).[47a,48,49] Rough criteria are obtained, which classify and characterize the interactions in question, after analysis of the plots for the typical interactions according to eqs 3−6.[47a,48,49] Scheme 2 shows the rough criteria, which are

Scheme 2. Rough Classification and Characterization of Interactions by θ and θ_p, Together with $k_b(\mathbf{r}_c)$

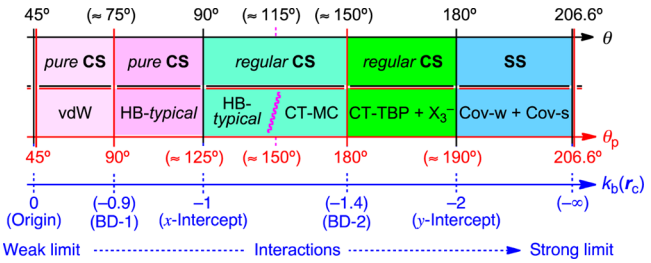

accomplished by the θ and θ_p values, together with $k_b(\mathbf{r}_c)$. The criteria will be employed to discuss the behavior of the E···E′ interactions in $\mathbf{1}^{\bullet+}$, $\mathbf{1}^{2+}$, and **1**, as a reference.

Methodological Details in Calculations. Neutral, radical cationic, and dicationic forms of **1** (**1**, $\mathbf{1}^{\bullet+}$, and $\mathbf{1}^{2+}$, respectively) were optimized using the Gaussian 09 program package.[51] Calculations are performed employing the 6-311+G(3df)[52] basis sets for O, S, and Se, the (7433111/743111/7411/2 + 1s1p1d1f) type[53] for Te, and the 6-311G+(d,p) basis sets for C and H at the Møller−Plesset second order energy correlation level (MP2),[54] after examination of the calculation method. Applicability of the basis set systems and levels was examined, employing the observed E···E distances of $\mathbf{1a}^{2+}$ (E = S) and $\mathbf{1d}^{2+}$ (E = Se), of which structures were determined by the X-ray crystallographic analysis. They were the **CC** form with substantial deformation[13] and the **CB** form,[14] respectively. Two basis set systems (BSSs) were examined. One is called BSS-A, which is the 6-311+G(3d) basis set for O, S, and Se with the 6-311+G(d,p) basis set for C and H (BSS-A). Another is BSS-B, which is the 6-311+G(3df) basis set for O, S, and Se with the 6-311+G(d,p) basis set for C and H. Various levels were also examined for MP2,[54] M06-2X,[55] M06,[55] LC-wPBE,[56] CAM-B3LYP,[57,58] and B3LYP.[59,60] The results for $\mathbf{1a}^{2+}$ and $\mathbf{1d}^{2+}$ are given in Tables S1 and S2 of the Supporting Information, respectively. A calculation method with BSS-B at the MP2 level is selected for the evaluations as mentioned above, since the magnitudes between the predicted and observed E···E′ distances seem to be less than 0.01 Å or around the value, although the counterions near the cationic species and/or the crystal packing effect are not considered in the examinations.[13,14,26] Unrestricted MP2 method (UMP2)[61] is applied to the odd electron system of $\mathbf{1}^{\bullet+}$. The structures were confirmed by the frequency analysis performed on the optimized structures.

QTAIM functions were calculated using the Gaussian 09 program package[51] with the same method of the optimizations. The results were analyzed with the AIM2000 program.[62] Normal coordinates of internal vibrations (NIV) obtained by the frequency analysis were employed to generate the perturbed structures.[49] A kth perturbed structure in question ($\mathbf{S}_{kw}$) is generated by the addition of the normal coordinates of the selected kth internal vibration ($\mathbf{N}_k$) to the standard orientation of a fully optimized structure ($\mathbf{S}_o$) in the matrix representation.[63] The motion of the selected internal vibration must be most effectively localized on the interaction in question. We call this method NIV, which is explained by eq 8. The coefficient f_{kw} in eq 8 is determined to satisfy eq 9, where r and r_o show the distances in the perturbed and fully optimized structures, respectively, with a_o of Bohr radius (0.529 18 Å).[47,48,64] Perturbed structures generated with NIV correspond to those with r in question being elongated or shortened by $0.05a_o$ or $0.1a_o$, relative to r_o (eq 9). The coefficient f_{kw} will be adjusted in this process. $\mathbf{N}_k$ of five digits are employed to predict $\mathbf{S}_{kw}$.[65]

$$\mathbf{S}_{kw} = \mathbf{S}_o + f_{kw} \cdot \mathbf{N}_k \quad (8)$$

$$r = r_o + wa_o(w = (0), \pm 0.05, \text{ and } \pm 0.1; \ a_o = 0.529\ 18\ \text{Å}) \quad (9)$$

$$y = a_o + a_1x + a_2x^2 + a_3x^3 \quad (R_c^2\text{: square of correlation coefficient}) \quad (10)$$

Each plot for an interaction with data of five points ($w = 0, \pm 0.05$, and ± 0.1) is analyzed by a regression curve assuming cubic function as shown in eq 10, where $(x, y) = (H_b(\mathbf{r}_c) - V_b(\mathbf{r}_c)/2, H_b(\mathbf{r}_c))$ ($R_c^2 > 0.999\ 99$ for usual situations).[66]

RESULTS AND DISCUSSION

Structural Feature in Neutral and Charged Forms of 1,5-Di(chalcogena)canes, 1, $\mathbf{1}^{\bullet+}$, and $\mathbf{1}^{2+}$. 1,5-Di(chalcogena)canes of the neutral, radical cationic, and dicationic forms, **1a**−**1j**, $\mathbf{1a}^{\bullet+}$−$\mathbf{1j}^{\bullet+}$, and $\mathbf{1a}^{2+}$−$\mathbf{1j}^{2+}$, are optimized with BSS-B at the MP2 level. Table 1 collects the E···E′, E−C_C, and E′−$C_{C'}$ distances (r(E, E′), r(E, C_C), r(E′, $C_{C'}$), respectively) for the **CB** forms of the optimized structures of **1a**−**1j**, $\mathbf{1a}^{\bullet+}$−$\mathbf{1j}^{\bullet+}$, and $\mathbf{1a}^{2+}$−$\mathbf{1j}^{2+}$, where C_C stands for the carbon atoms adjacent to E and E′ in the chair ring. The notation, containing points M and M′, is illustrated in the footnote of Table 1, modeled by $\mathbf{1}^{2+}$.

It would be instructive to compare the r(E, E′) values of **1a**−**1j**, $\mathbf{1a}^{\bullet+}$−$\mathbf{1j}^{\bullet+}$, and $\mathbf{1a}^{2+}$−$\mathbf{1j}^{2+}$ with the corresponding values of **2a**−**2j**. Therefore, the Δr(E, E′) values [=r(E, E′: **1***x*∗) − r(E, E′: **2***x*); ***x*** = **a**−**j** and ∗ = null, •+, and 2+] are also shown in Table 1, where r(E, E′: **2***x*) are expected to be very close to the sum of covalent radii of E and E′ (r_{cov}(E) + r_{cov}(E′)). Table 1 also collects the angles (∠E′EM and ∠EE′M′) and torsional angles (ϕ(MEE′M′)) for **1a**−**1j**, $\mathbf{1a}^{\bullet+}$−$\mathbf{1j}^{\bullet+}$, and $\mathbf{1a}^{2+}$−$\mathbf{1j}^{2+}$, where a point M is put at the midpoint between C_C and C_B, adjacent to E and a point M′ at the midpoint between $C_{C'}$ and $C_{B'}$, adjacent to E′ (see footenote of Table 1).

Figure 5 shows the plot of r(E, E′) for **1a**−**1j**, $\mathbf{1a}^{\bullet+}$−$\mathbf{1j}^{\bullet+}$, and $\mathbf{1a}^{2+}$−$\mathbf{1j}^{2+}$, together with **2a**−**2j**. The r(E, E′) values for **2a**−**2j** increase in the order **2g** < **2h** < **2i** < **2j** < **2a** < **2b** < **2d** < **2c** < **2e** < **2f**, where the order seems irregular around **2d** and **2c** (see, Figure 5 and Table 1). The r(E, E′) values of $\mathbf{1a}^{2+}$−$\mathbf{1j}^{2+}$ are very

DOI: 10.1021/acs.joc.5b01794
J. Org. Chem. 2015, 80, 11963−11976

Table 1. Distances, Angles, and Torsional Angles for Neutral and Charged Forms of *cyclo*-E($CH_2CH_2CH_2$)$_2$E′ (1) (CB), Together with Relative Energies, Optimized with BSS-B at the MP2 Level[a]

species (E, E′)	r(E, E′) (Å)	Δr(E, E′)[b] (Å)	r(E, C_C)[c] (Å)	r(E, C_B)[d] (Å)	∠E′EM (deg)	∠EE′M′ (deg)	ϕ(MEE′M′) (deg)	ΔE[e] (eV)	symmetry
Neutral Species									
1a (S, S)	3.4093	1.3270	1.8172	1.8172	69.7	69.7	0.0	as 0.00	C_s
1b (S, Se)	3.7499	1.5081	1.8160	1.9510	72.1	39.5	11.4	as 0.00	C_1
1c (S, Te)	3.7372	1.3243	1.8185	2.1495	78.3	41.4	11.3	as 0.00	C_1
1d (Se, Se)	3.5740	1.0422	1.9555	1.9555	67.5	67.5	0.0	as 0.00	C_s
1e (Se, Te)	3.8176	1.2769	1.9808	2.2062	78.5	45.0	11.9	as 0.00	C_1
1f (Te, Te)	3.8244	1.0946	2.1541	2.1541	47.4	46.4	0.0	as 0.00	C_s
1g (O, O)	2.8557	1.3941	1.4211	1.4211	79.6	79.6	0.0	as 0.00	C_s
1h (O, S)	3.0965	1.3965	1.4206	1.8172	91.3	61.2	−0.5	as 0.00	C_1
1i (O, Se)	3.1740	1.3292	1.4209	1.9546	96.1	54.8	1.8	as 0.00	C_1
1j (O, Te)	3.2475	1.2497	1.4216	2.1511	103.8	47.4	2.8	as 0.00	C_1
Radical Cationic Species									
1a$^{\bullet+}$ (S, S)	2.7049	0.6226	1.8145	1.8145	85.8	85.8	0.0	6.81	C_s
1b$^{\bullet+}$ (S, Se)	2.7783	0.5365	1.8180	1.9522	88.3	80.7	−0.4	6.69	C_1
1c$^{\bullet+}$ (S, Te)	2.9068	0.4939	1.8216	2.1439	92.4	72.7	−0.5	6.47	C_1
1d$^{\bullet+}$ (Se, Se)	2.8730	0.5059	1.9552	1.9552	82.7	82.7	0.0	6.53	C_s
1e$^{\bullet+}$ (Se, Te)	3.0094	0.4687	1.9587	2.1465	86.3	74.6	−0.1	6.26	C_1
1f$^{\bullet+}$ (Te, Te)	3.1814	0.4516	2.1504	2.1504	77.6	77.6	0.0	6.09	C_s
1g$^{\bullet+}$ (O, O)	2.3546	0.8930	1.4118	1.4118	95.1	95.1	0.0	8.35	C_s
1h$^{\bullet+}$ (O, S)	2.3410	0.6410	1.4470	1.8014	115.1	78.7	−3.0	7.49	C_1
1i$^{\bullet+}$ (O, Se)	2.4232	0.5784	1.4462	1.9419	118.2	73.1	−3.6	7.25	C_1
1j$^{\bullet+}$ (O, Te)	2.5096	0.5118	1.4479	2.1333	124.3	66.0	−5.8	6.80	C_1
Dicationic Species									
1a^{2+} (S, S)	2.1373	0.0550	1.8353	1.8353	99.0	99.0	0.0	18.16	C_s
1b^{2+} (S, Se)	2.2619	0.0201	1.8398	1.9712	99.5	92.4	−1.3	17.87	C_1
1c^{2+} (S, Te)	2.4513	0.0384	1.8482	2.1476	99.7	84.5	−2.2	17.36	C_1
1d^{2+} (Se, Se)	2.3770	0.0099	1.9768	1.9768	93.3	93.3	0.0	17.54	C_s
1e^{2+} (Se, Te)	2.5592	0.0185	1.9856	2.1536	93.7	85.7	−1.2	16.97	C_1
1f^{2+} (Te, Te)	2.7504	0.0206	2.1639	2.1639	86.1	86.1	0.0	16.53	C_s
1g^{2+} (O, O)	2.3257	0.8641	1.4054	1.4054	95.2	95.2	0.0	21.72	C_s
1h^{2+} (O, S)	1.7271	0.0271	1.5616	1.8030	131.2	97.0	−0.7	19.62	C_1
1i^{2+} (O, Se)	1.8690	0.0242	1.5479	1.9419	130.0	89.7	−3.9	19.26	C_1
1j^{2+} (O, Te)	2.0396	0.0418	1.5373	2.1199	131.5	80.9	−5.4	18.42	C_1

[a]For BSS-B: The 6-311+G(3df) basis set for O, S, and Se and that of the (7433111/743111/7411/2 + 1s1p1d1f) type for Te with the 6-311+G(d,p) basis set for C and H. [b]Δr(E, E′) = r(E, E′: **1***x*∗) − r(E, E′: **2***x*), where ***x*** = **a**−**j** and ∗ = null, •+, and 2+. [c]r(E, C_C) = r(E′, $C_{C'}$). [d]r(E, C_B) = r(E′, $C_{B'}$). [e]ΔE = E (**1***x*∗) − E (**1***x*), where ***x*** = **a**−**j** and ∗ = •+ and 2+.

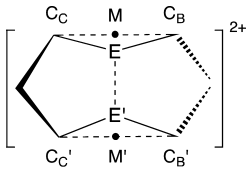

close to the corresponding values of **2a**−**2j**, except for **1g**$^{2+}$ (O, O). The Δr(O, O) value of 0.86 Å for **1g**$^{2+}$ is only slightly less than Δr(O, O) for **1g**$^{\bullet+}$ (0.89 Å), where Δr(E, E′) values are 0.01−0.06 Å for **1a**$^{2+}$−**1j**$^{2+}$, except for **1g**$^{2+}$. The E···E′ σ(2c−2e) interactions in **1a**$^{2+}$−**1j**$^{2+}$ must be very close to the corresponding interactions in **2a**−**2j**, respectively, except for that in **1g**$^{2+}$ (O, O) versus **2g** (O, O). The O···O interaction in **1g**$^{2+}$ (O, O) must be analyzed carefully. The plot for **1a**$^{\bullet+}$−**1j**$^{\bullet+}$ seems parallel to that of **2a**−**2j**, although the data for **1g**$^{\bullet+}$ (O, O) deviate somewhat from what is expected (Figure 5). The Δr(E, E′) values are 0.45−0.64 Å for **1a**$^{\bullet+}$−**1f**$^{\bullet+}$ and **1h**$^{\bullet+}$−**1j**$^{\bullet+}$, although Δr(E, E′) = 0.89 Å for **1g**$^{\bullet+}$. The value for **1g**$^{\bullet+}$ is somewhat larger than the value of 0.78 Å for HOOH$^{\bullet-}$.[50]

The plot for **1a**−**1j** seems almost parallel to that of **2a**−**2j** (Figure 5). The Δr(E, E′) values are predicted to be 1.04−1.51 Å for σ(2c−4e) in **1a**−**1j**, where the values are small for **1d** (Se, Se) (1.04 Å) and **1f** (Te, Te) (1.10 Å) but large for **1b** (S, Se) (1.51 Å). The disadvantageous conditions are suggested for S···Se of **1b**. Indeed, the large values must be the reflection of the weak E···E′ transannular interactions, but some sterically disadvantageous conditions must also be important for the predicted values. The Δr(E, E′) values of σ(2c−4e) in **1a**−**1j** (1.04−1.51 Å) decrease in the formation of σ(2c−3e) in **1a**$^{\bullet+}$−**1f**$^{\bullet+}$, with values of 0.45−0.64 Å and 0.89 Å for **1g**$^{\bullet+}$ (O, O). The values become much smaller for the formation of σ(2c−2e) in **1a**$^{2+}$−**1j**$^{2+}$ (0.01−0.06 Å), except for **1g**$^{2+}$ (O, O) (0.86 Å). The behavior of E···E′ σ(2c−2e) in **1a**$^{2+}$−**1j**$^{2+}$ must be very close to that in **2a**−**2j**, except for **1g**$^{2+}$ (O, O) versus **2g** (O, O).

The ∠E′EM and ∠EE′M′ values are closely related to the directions of n_p(E) and n_p(E′) toward E′ and E, respectively. They will overlap effectively if the angles are close to 90°. While ∠E′EM and ∠EE′M′ in **1a**$^{2+}$−**1g**$^{2+}$ are 86°−100° and 85°−99°,

DOI: 10.1021/acs.joc.5b01794
J. Org. Chem. 2015, 80, 11963−11976

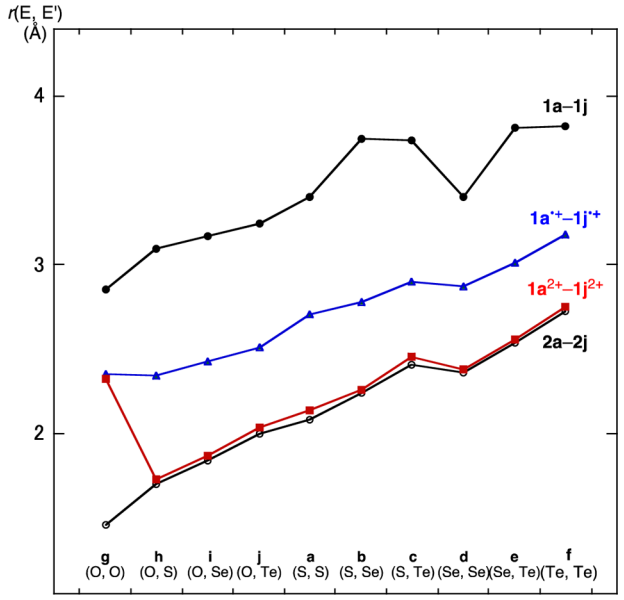

Figure 5. Plots of r(E, E′) for **1a**−**1j**, $\mathbf{1a}^{\bullet+}$−$\mathbf{1j}^{\bullet+}$, and $\mathbf{1a}^{2+}$−$\mathbf{1j}^{2+}$, together with **2a**−**2j**.

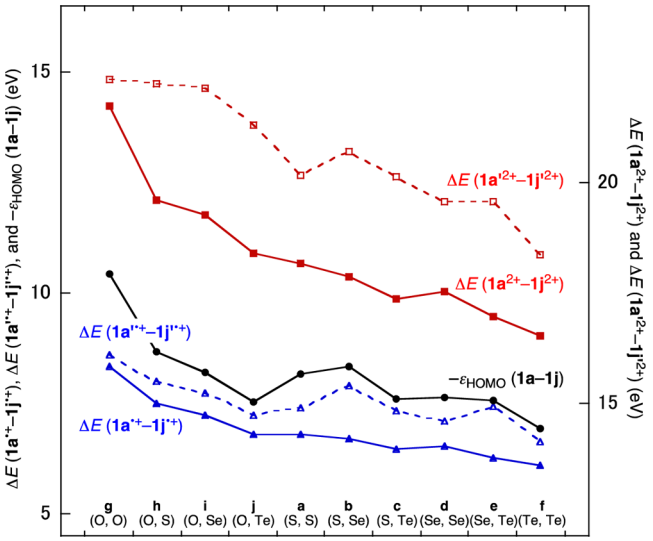

Figure 6. Plots of ΔE ($\mathbf{1a}^{\bullet+}$−$\mathbf{1j}^{\bullet+}$) (blue ▲), ΔE ($\mathbf{1a}'^{\bullet+}$−$\mathbf{1j}'^{\bullet+}$) (blue △), ΔE ($\mathbf{1a}^{2+}$−$\mathbf{1j}^{2+}$) (red ■), ΔE ($\mathbf{1a}'^{2+}$−$\mathbf{1j}'^{2+}$) (red □), and $-\varepsilon_{HOMO}$ (**1a**−**1j**) (black ●). The solid lines connect the energies or energy differences for the optimized structures, whereas the dotted lines connect those evaluated employing the optimized structures of **1a**−**1j**.

respectively, those in $\mathbf{1h}^{2+}$−$\mathbf{1j}^{2+}$ are 130°−132° and 81°−97°, respectively. The values are the desirable range of around 90°, except for ∠E′EM in $\mathbf{1h}^{2+}$−$\mathbf{1j}^{2+}$. Similarly, ∠E′EM and ∠EE′M′ in $\mathbf{1a}^{\bullet+}$−$\mathbf{1g}^{\bullet+}$ are 77°−95° and 72°−95°, respectively, whereas those in $\mathbf{1h}^{\bullet+}$−$\mathbf{1j}^{\bullet+}$ are 115°−125° and 66°−79°, respectively. The values seem acceptable. ∠E′EM in $\mathbf{1h}^{2+}$−$\mathbf{1j}^{2+}$ of 130°−132° are larger than 90° by over 40°, which seem too large to be accepted at first glance, although the differences are less than 45°. While ∠E′EM (=∠EE′M′) values for **1a** (S, S), **1d** (Se, Se), and **1g** (O, O) are close to 70°, 70°, and 80°, respectively, that for **1f** (Te, Te) is 47° on average. On the other hand, ∠EE′M′ for **1b** (S, Se) is close to 39.5°, which is the smallest as shown in Table 1. Some ∠E′EM and/or ∠EE′M′ values seem smaller than the acceptable range for **1a**−**1j**. The disadvantageous geometry for the S···Se interaction in **1b** must decrease the effective overlap between the p-type lone pair orbitals of S and Se. On the other hand, the values for the torsional angle ϕ(MEE′M′) are less than 12° for all the species.

How are the energies in the formation of the radical cations ($\mathbf{1a}^{\bullet+}$−$\mathbf{1j}^{\bullet+}$) and dications ($\mathbf{1a}^{2+}$−$\mathbf{1j}^{2+}$) from the corresponding neutral species (**1a**−**1j**)? The ΔE values are evaluated for $\mathbf{1a}^{\bullet+}$−$\mathbf{1j}^{\bullet+}$ [ΔE ($\mathbf{1a}^{\bullet+}$−$\mathbf{1j}^{\bullet+}$) = E ($\mathbf{1a}^{\bullet+}$−$\mathbf{1j}^{\bullet+}$) − E (**1a**−**1j**)] and $\mathbf{1a}^{2+}$−$\mathbf{1j}^{2+}$ [ΔE ($\mathbf{1a}^{2+}$−$\mathbf{1j}^{2+}$) = E ($\mathbf{1a}^{2+}$−$\mathbf{1j}^{2+}$) − E (**1a**−**1j**)], using the E values in Table 1. Similarly, ΔE ($\mathbf{1a}'^{\bullet+}$−$\mathbf{1j}'^{\bullet+}$) [= E ($\mathbf{1a}'^{\bullet+}$−$\mathbf{1j}'^{\bullet+}$) − E (**1a**−**1j**)] and ΔE ($\mathbf{1a}'^{2+}$−$\mathbf{1j}'^{2+}$) [= E ($\mathbf{1a}'^{2+}$−$\mathbf{1j}'^{2+}$) − E (**1a**−**1j**)] are also evaluated, where E ($\mathbf{1a}'^{\bullet+}$−$\mathbf{1j}'^{\bullet+}$) and E ($\mathbf{1a}'^{2+}$−$\mathbf{1j}'^{2+}$) stand for the energies of the radical cations and dications evaluated employing the fully optimized structures of **1a**−**1j**. The ΔE ($\mathbf{1a}^{\bullet+}$−$\mathbf{1j}^{\bullet+}$), ΔE ($\mathbf{1a}^{2+}$−$\mathbf{1j}^{2+}$), ΔE ($\mathbf{1a}'^{\bullet+}$−$\mathbf{1j}'^{\bullet+}$), ΔE ($\mathbf{1a}'^{2+}$−$\mathbf{1j}'^{2+}$), and $-\varepsilon_{HOMO}$ (**1a**−**1j**) values are collected in Table S3 in the Supporting Information, together with the differences between them. Figure 6 shows the plot of ΔE ($\mathbf{1a}^{\bullet+}$−$\mathbf{1j}^{\bullet+}$), ΔE ($\mathbf{1a}^{2+}$−$\mathbf{1j}^{2+}$), ΔE ($\mathbf{1a}'^{\bullet+}$−$\mathbf{1j}'^{\bullet+}$), ΔE ($\mathbf{1a}'^{2+}$−$\mathbf{1j}'^{2+}$), and $-\varepsilon_{HOMO}$ (**1a**−**1j**). The $\Delta\varepsilon_{HOMO}$ ($\mathbf{1a}'^{\bullet+}$−$\mathbf{1j}'^{\bullet+}$) values in Table S3 correspond to the differences between $-\varepsilon_{HOMO}$ (**1a**−**1j**) and ΔE ($\mathbf{1a}'^{\bullet+}$−$\mathbf{1j}'^{\bullet+}$) in Figure 6 (for the longitudinal axis direction).

Each of the species $\mathbf{1a}'^{\bullet+}$−$\mathbf{1j}'^{\bullet+}$ is stabilized through the redistribution of the remaining electrons after the removal of an electron from each of **1a**−**1j**, in the same structure, which is estimated to be 0.13−1.83 eV through $\Delta\varepsilon_{HOMO}$ ($\mathbf{1a}'^{\bullet+}$−$\mathbf{1j}'^{\bullet+}$) [=−ε_{HOMO} (**1a**−**1j**) − ΔE ($\mathbf{1a}'^{\bullet+}$−$\mathbf{1j}'^{\bullet+}$)]. The stabilization energies for $\mathbf{1a}^{\bullet+}$−$\mathbf{1j}^{\bullet+}$ from $\mathbf{1a}'^{\bullet+}$−$\mathbf{1j}'^{\bullet+}$ through the structural change with the redistribution of the remaining electrons after one-electron removal are also estimated by $\Delta\Delta E$ ($\mathbf{1a}'^{\bullet+}$−$\mathbf{1j}'^{\bullet+}$) of 0.25−1.21 eV. Similarly, the stabilization energies for $\mathbf{1a}^{2+}$−$\mathbf{1j}^{2+}$ from $\mathbf{1a}'^{2+}$−$\mathbf{1j}'^{2+}$ through the structural change with the redistribution of the remaining electrons are estimated to be 0.61−2.89 eV by $\Delta\Delta E$ ($\mathbf{1a}'^{2+}$−$\mathbf{1j}'^{2+}$), which occur after two-electron removal from each of the species **1a**−**1j**.

Figure 7 shows the plot of ΔE ($\mathbf{1a}'^{\bullet+}$−$\mathbf{1j}'^{\bullet+}$) versus $-\varepsilon_{HOMO}$, which is well-analyzed by dividing the data into three groups: Data from **a** (S, S), **d** (Se, Se), and **f** (Te, Te) make group **I**

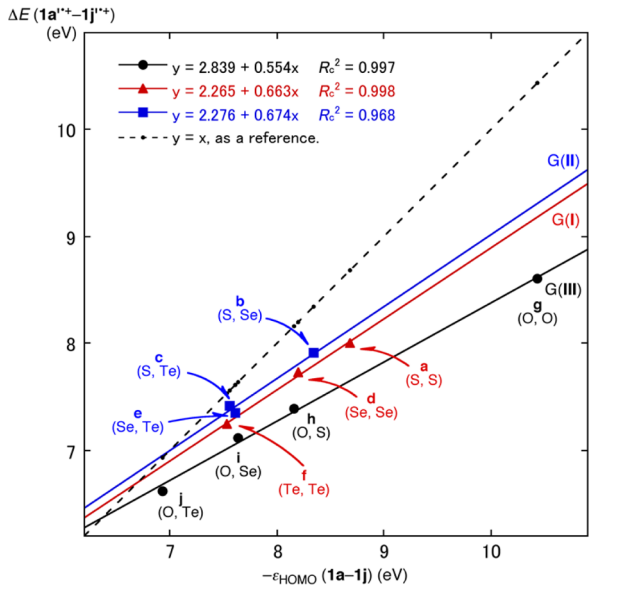

Figure 7. Plots of ΔE ($\mathbf{1a}'^{\bullet+}$−$\mathbf{1j}'^{\bullet+}$) versus $-\varepsilon_{HOMO}$ (**1a**−**1j**), which are analyzed as three correlations.

DOI: 10.1021/acs.joc.5b01794
J. Org. Chem. 2015, 80, 11963−11976

(G(**I**)), those of **b** (S, Se), **c** (S, Te), and **e** (Se, Te) are group **II** (G(**II**)), and those of **g** (O, O), **h** (O, S), **i** (O, Se), and **j** (O, Te) belong to group **III** (G(**III**)). The correlations are given in the figure. The removal of an electron and the redistribution of the remaining electrons will occur equally on E and E′ in G(**I**). The properties of E would be close to those of E′ in G(**II**); therefore, the process is expected to occur not equally but not so differently on E and E′. As a result, the behavior in G(**II**) would be different from that in G(**I**), although slightly. The mechanism in G(**III**) would be substantially different from that in G(**I**) and G(**II**). The process for the removal of an electron and the redistribution of the remaining electrons would hardly occur on E = O in G(**III**), where (E, E′) = (O, O) also belongs to G(**III**).

The plot of ΔE (**1a**$^{\bullet+}$−**1j**$^{\bullet+}$) versus $-\varepsilon_{HOMO}$ is drawn in Figure S1 of the Supporting Information, which is very similar to that shown in Figure 7. The plot in Figure S1 is similarly analyzed as three correlations. The correlations are shown in Table S4 of the Supporting Information (entries 1−3). The plot of ΔE (**1a**$^{\bullet+}$−**1j**$^{\bullet+}$) versus ΔE (**1a′**$^{\bullet+}$−**1j′**$^{\bullet+}$) is similarly shown in Figure S2 of the Supporting Information. A good correlation is obtained for G(**I**) + G(**III**), although data of G(**II**) deviate from the correlation. The correlation is given in Table S4 (entry 4). The plot of ΔE (**1a**$^{2+}$−**1j**$^{2+}$) versus ΔE (**1a**$^{\bullet+}$−**1j**$^{\bullet+}$) is displayed in Figure S3 of the Supporting Information. The plot is well-analyzed as a correlation without deviation, which is given in Table S4 (entry 5). It is worthwhile to comment that ΔE (**1a**$^{2+}$−**1j**$^{2+}$) values are well-correlated to ΔE (**1a**$^{\bullet+}$−**1j**$^{\bullet+}$), irrespective of the irregular behavior of r(O, O) in **1g**$^{2+}$.

Survey of the E···E′ Interactions in 1, 1$^{\bullet+}$, and 1^{2+}. The E···E′ interactions are surveyed as exemplified by E = E′ = Se in the **CB** structures of **1**, **1**$^{\bullet+}$, and **1**$^{2+}$, which are denoted by **1d** (**CB**), **1d**$^{\bullet+}$ (**CB**), and **1d**$^{2+}$ (**CB**), respectively. The structures are optimized retaining the C_s symmetry; therefore, the E···E′ interactions can be easily visualized. Figure 8 draws energy diagrams of ψ_{54}−ψ_{59} for **1d** (**CB**), **1d**$^{\bullet+}$ (**CB**), and **1d**$^{2+}$ (**CB**). HOMO−4, HOMO−3, HOMO−2, HOMO−1, HOMO, and LUMO correspond to **1d** (**CB**), $\psi_{54}(\alpha)$−$\psi_{59}(\alpha)$ and $\psi_{54}(\beta)$−$\psi_{59}(\beta)$ to **1d**$^{\bullet+}$ (**CB**), and HOMO−3, HOMO−2, HOMO−1, HOMO, LUMO, and LUMO+1 to **1d**$^{2+}$ (**CC**). Each $\psi_i(\alpha)$ is more stable than $\psi_i(\beta)$ in **1**$^{\bullet+}$, since the number of α-spin electrons is assumed to be larger than that of β-spin electrons by one, resulting in the larger contribution from the exchange integrals between the α-spin electrons to the α-spin MO energies. Consequently, ψ_{58} (HOMO) of **1d** (**CB**) will split into $\psi_{58}(\alpha)$ and $\psi_{58}(\beta)$ in **1d**$^{\bullet+}$ (**CB**), after removal of an electron from **1d** (**CB**). In this case, $\psi_{58}(\alpha)$ and $\psi_{58}(\beta)$ have the characters of HOMO and LUMO, respectively, although $\psi_{58}(\alpha)$ should be called SOMO (singly occupied molecular orbital).

Figure 9 shows ψ_{57}(HOMO−1) and ψ_{58}(HOMO) of **1d** (**CB**), ψ_{57}(β: HOMO−1: SOMO) and ψ_{58}(α: HOMO: SOMO) of **1d**$^{\bullet+}$ (**CB**), and ψ_{54}(HOMO−3) and ψ_{58}(LUMO) of **1d**$^{2+}$ (**CB**). The Se···Se interactions in ψ_{58}(HOMO) of **1d** (**CB**), ψ_{58}(α: HOMO) of **1d**$^{\bullet+}$ (**CB**), and ψ_{58}(LUMO) of **1d**$^{2+}$ (**CB**) have the n_p(Se) − n_p(Se) character, whereas those in ψ_{57}(HOMO−1) of **1d** (**CB**), ψ_{57}(β: HOMO−1) of **1d**$^{\bullet+}$ (**CB**), and ψ_{54}(HOMO−3) of **1d**$^{2+}$ (**CB**) have the n_p(Se) + n_p(Se) character. One may expect that the typical interactions of the n_p(Se) + n_p(Se) character should appear in the HOMO for **1d**$^{2+}$ (**CB**), at first glance. However, the character in **1d**$^{2+}$ (**CB**) is not predicted for HOMO but

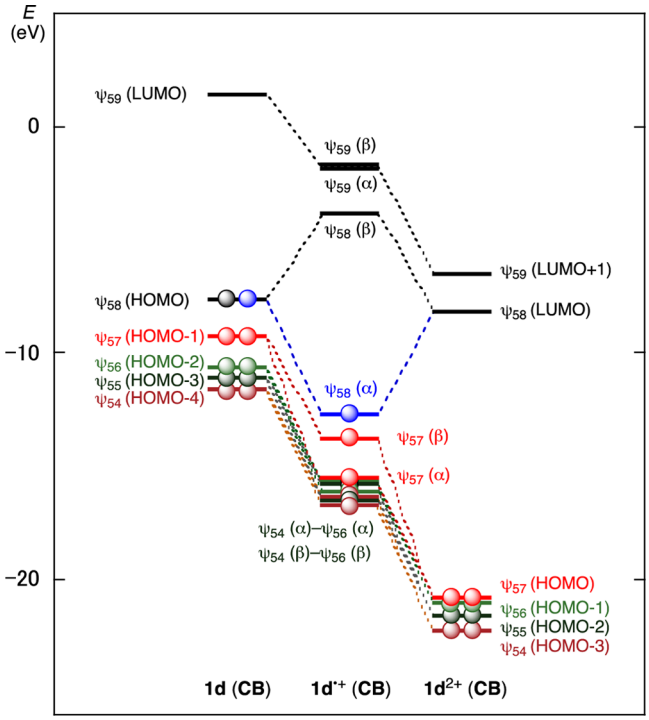

Figure 8. Energy diagram, drawn as exemplified by **1d** (**CB**), **1d**$^{\bullet+}$ (**CB**), and **1d**$^{2+}$ (**CB**).

mainly for HOMO−3 by the MP2 calculations. The n_p(Se) orbitals in **1d**$^{2+}$ (**CB**) are so stabilized, due to the high positive charge developed on each Se (Qn(Se) = 0.877), that they interact with MOs of the CH_2 groups. Consquently, the MO character of the n_p(Se) + n_p(Se) type will spread over not only HOMO−3 but also HOMO−2, and HOMO−1 in **1d**$^{2+}$ (**CB**), although not shown.

The Se-*-Se interactions in **1d** (**CB**), **1d**$^{\bullet+}$ (**CB**), and **1d**$^{2+}$ (**CB**) can be explained by the σ(2c−4e), σ(2c−3e), and σ(2c−2e) models, respectively (cf., Figure 3 for the E···E′ interactions in **1**, **1**$^{\bullet+}$, and **1**$^{2+}$). It must be difficult for the E···E′ interactions in **1** to stabilize through the orbital overlaps, due to the high disadvantageous exchange repulsive factors of σ(2c−4e). On the other hand, the E···E′ σ(2c−2e) interactions in **1**$^{2+}$ will be much stabilized through the orbital overlaps due to the advantageous exchange factors. The E···E′ σ(2c−3e) interactions in **1**$^{\bullet+}$ must be intermediate between σ(2c−4e) in **1** and σ(2c−2e) in **1**$^{2+}$.

After clarifying the basic structural feature, QTAIM-DFA is applied to the E---E′ interactions in **1a**−**1j**, **1a**$^{\bullet+}$−**1j**$^{\bullet+}$, and **1a**$^{2+}$−**1j**$^{2+}$, next.

Molecular Graphs, Contour Plots, Negative Laplacians, and Trajectory Plots Around the E-*-E′ Interactions. Figure 10 shows the molecular graphs, exemplified by **1d** (**CB**), **1d**$^{\bullet+}$ (**CB**), and **1d**$^{2+}$ (**CB**). All BCPs expected are detected, containing those between the Se-*-Se atoms. Figure 11 shows the contour plots, exemplified by **1d** (**CB**), **1d**$^{\bullet+}$ (**CB**), and **1d**$^{2+}$ (**CB**). The maps are drawn on the planes constructed by the C−Se−Se−C atoms in **1d** (**CB**), **1d**$^{\bullet+}$ (**CB**), and **1d**$^{2+}$ (**CB**), where two Se atoms, two C atoms, a BCP on the Se-*-Se interation, and two BCPs on the Se−C bonds are located on each plane. The contour plots for **1d** (**CB**), **1d**$^{\bullet+}$ (**CB**), and **1d**$^{2+}$ (**CB**) create the characteristic Se-*-Se interactions of the σ(2c−4e), σ(2c−3e), and σ(2c−2e) types, respectively.

DOI: 10.1021/acs.joc.5b01794
J. Org. Chem. 2015, 80, 11963−11976

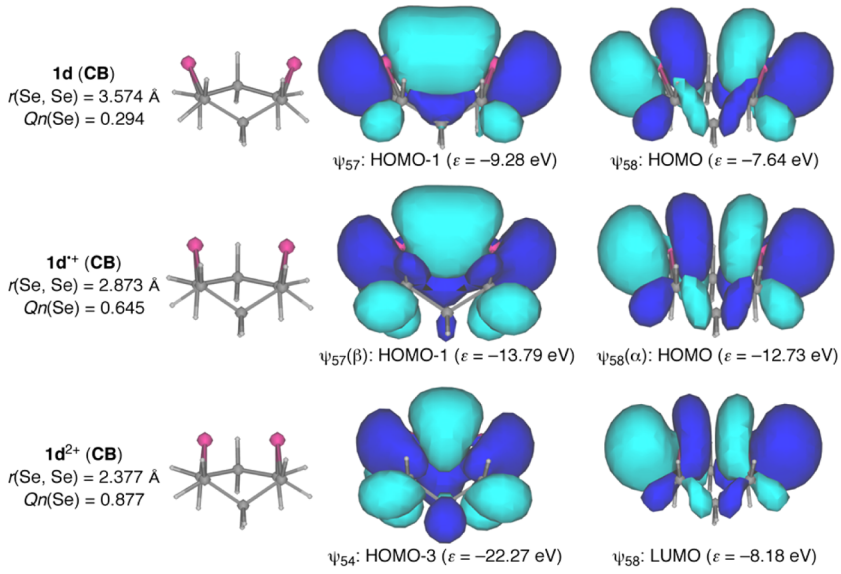

Figure 9. Typical $n_p(Se)\cdots n_p(Se)$ interactions in **1** (**CB**), $\mathbf{1}^{\bullet+}$ (**CB**), and $\mathbf{1}^{2+}$ (**CB**). Orbital energies, distances of Se···Se, and charges developed on Se are also given.

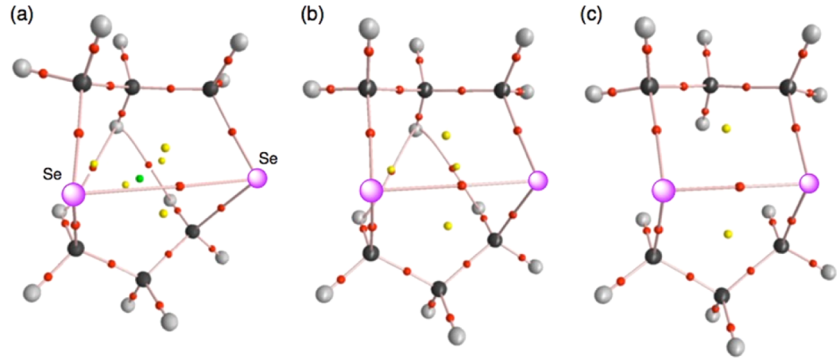

Figure 10. Molecular graphs for **1d** (**CB**) (a), $\mathbf{1d}^{\bullet+}$ (**CB**) (b), and $\mathbf{1d}^{2+}$ (**CB**) (c). Bond paths are denoted by solid lines, and BCPs are denoted by small red balls on the bond path, together with ring critical points (small yellow balls) and cage critical points (small lime green balls).

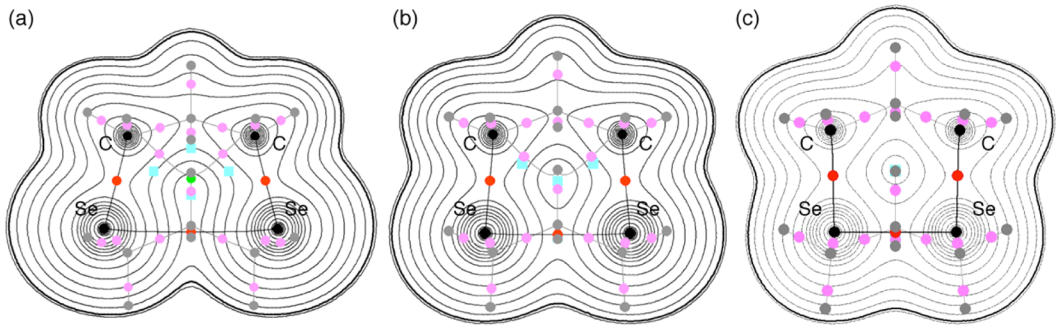

Figure 11. Contour plots of $\rho_b(\mathbf{r}_c)$ drawn on the C−Se−Se−C plane for **1d** (**CB**) (a), $\mathbf{1d}^{\bullet+}$ (**CB**) (b), and $\mathbf{1d}^{2+}$ (**CB**) (c), together with BCPs (red solid circles on the plane and pink solid circles out of the plane), ring critical points (cyan solid squares out of the plane), cage critical points (lime green solid circles), critical points of $(\omega, \sigma) = (3, -3)$ (corresponding to atoms: black solid circles on the plane and gray solid circles out of the plane), and bond paths. The contours (ea_o^{-3}) are at 2^l ($l = \pm 8, \pm 7, \ldots, 0$) and 0.0047 (heavy line).

Figure 12 shows negative Laplacians, exemplified by **1d** (**CB**), $\mathbf{1d}^{\bullet+}$ (**CB**), and $\mathbf{1d}^{2+}$ (**CB**). The BCPs between Se-∗-Se of **1d** (**CB**) and $\mathbf{1d}^{\bullet+}$ (**CB**) exist in the blue area, whereas that of $\mathbf{1d}^{2+}$ (**CB**) is in the red area, which means that the Se-∗-Se interactions are classified as the CS interactions for the former two, whereas that of the latter is classified as the SS interactions. Trajectory plots are similarly drawn for **1d** (**CB**), $\mathbf{1d}^{\bullet+}$ (**CB**), and $\mathbf{1d}^{2+}$ (**CB**) in Figure S5 of the Supporting Information, where each space around the species are well fractionalized to the atoms. Figure S6 of the Supporting Information depicts the Se···Se stretching modes of **1d** (**CB**), $\mathbf{1d}^{\bullet+}$ (**CB**), and $\mathbf{1d}^{2+}$ (**CB**), necessary to generate the perturbed structures around the fully optimized structures, for example.

QTAIM-DFA Parameters of (R, θ) and (θ_p, κ_p), Evaluated for E-∗-E′ in 1, $\mathbf{1}^{\bullet+}$, and $\mathbf{1}^{2+}$. QTAIM functions are calculated for $\rho_b(\mathbf{r}_c)$, $H_b(\mathbf{r}_c) - V_b(\mathbf{r}_c)/2$, $H_b(\mathbf{r}_c)$, and $k_b(\mathbf{r}_c)$

DOI: 10.1021/acs.joc.5b01794
J. Org. Chem. 2015, 80, 11963−11976

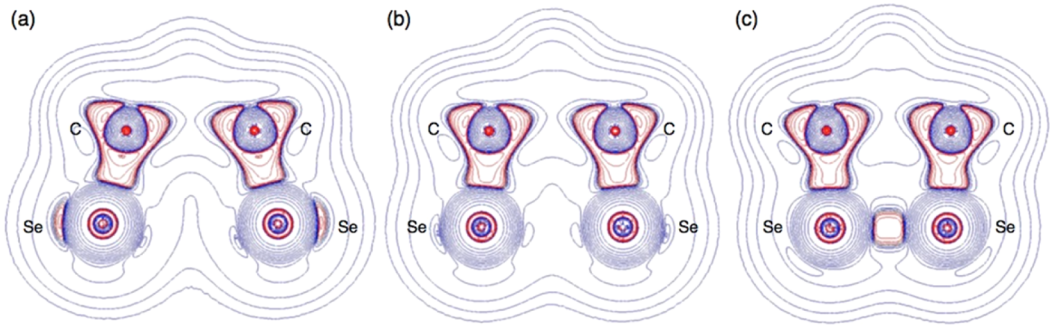

Figure 12. Negative Laplacians drawn on the C−Se−Se−C plane for **1d** (**CB**) (a), **1d**$^{\bullet+}$ (**CB**) (b), and **1d**$^{2+}$ (**CB**) (c), where the negative areas are shown in red and positive areas in blue.

Table 2. QTAIM Functions and Parameters Evaluated for the Neutral, Radical Cationic, and Dicationic Forms in *cyclo*-E(CH$_2$CH$_2$CH$_2$)$_2$E′ (1) Calculated Employing QTAIM-DFA with NIV at the MP2 Level[a]

interaction (E-∗-E′)	$\rho_b(\mathbf{r}_c)$ (au)	$c\nabla^2\rho_b(\mathbf{r}_c)$[b] (au)	$H_b(\mathbf{r}_c)$ (au)	$k_b(\mathbf{r}_c)$[c]	R (au)	θ (deg)	ν_n (n)[d] (cm^{-1})	k_f[d] (mdyn Å^{-1})	θ_p (deg)	κ_p (au^{-1})
				Neutral Species						
S-∗-S/**1a**	0.0130	0.0043	0.0002	−0.973	0.0043	87.0	146.6 (2)	0.087	113.2	127
S-∗-Se/**1b**	*e*	*e*	*e*	*e*	*e*	*e*	*e*	*e*	*e*	*e*
S-∗-Te/**1c**	0.0106	0.0032	0.0003	−0.954	0.0032	84.9	59.7 (1)	0.009	170.8	0.0
Se-∗-Se/**1d**	0.0127	0.0036	0.0002	−0.969	0.0036	86.6	97.4 (2)	0.089	110.3	178
Se-∗-Te/**1e**	0.0106	0.0029	0.0002	−0.967	0.0029	86.4	54.9 (1)	0.014	142.1	0.0
Te-∗-Te/**1f**	0.0133	0.0027	−0.0003	−1.060	0.0027	97.3	77.8 (2)	0.077	121.0	259
O-∗-O/**1g**	0.0130	0.0058	0.0000	−0.998	0.0058	89.8	196.7 (2)	0.131	92.6	199
O-∗-S/**1h**	0.0135	0.0052	0.0000	−0.996	0.0052	89.5	190.9 (3)	0.111	101.8	38.3
O-∗-Se/**1i**	0.0130	0.0048	0.0001	−0.987	0.0048	88.5	169.5 (3)	0.076	102.5	21.1
O-∗-Te/**1j**	0.0138	0.0045	−0.0003	−1.029	0.0045	93.4	150.5 (3)	0.080	104.1	37.9
				Radical Cationic Species						
S-∗-S/**1a**$^{\bullet+}$	0.0472	0.0074	−0.0075	−1.338	0.0105	135.6	253.9 (4)	0.284	162.3	43.1
S-∗-Se/**1b**$^{\bullet+}$	0.0464	0.0062	−0.0083	−1.400	0.0103	143.1	222.8 (4)	0.231	165.8	89.7
S-∗-Te/**1c**$^{\bullet+}$	0.0441	0.0043	−0.0092	−1.516	0.0102	154.9	184.1 (3)	0.099	177.3	4.8
Se-∗-Se/**1d**$^{\bullet+}$	0.0439	0.0052	−0.0080	−1.434	0.0096	146.9	173.6 (3)	0.344	175.7	26.6
Se-∗-Te/**1e**$^{\bullet+}$	0.0417	0.0038	−0.0083	−1.524	0.0091	155.5	154.9 (3)	0.373	179.8	50.4
Te-∗-Te/**1f**$^{\bullet+}$	0.0385	0.0028	−0.0072	−1.563	0.0077	158.8	129.0 (2)	0.069	181.6	54.3
O-∗-O/**1g**$^{\bullet+}$	0.0323	0.0162	0.0035	−0.879	0.0166	77.8	176.9 (2)	0.125	77.6	24.5
O-∗-S/**1h**$^{\bullet+}$	0.0547	0.0150	−0.0065	−1.178	0.0164	113.4	295.1 (4)	0.138	135.6	60.9
O-∗-Se/**1i**$^{\bullet+}$	0.0500	0.0130	−0.0070	−1.213	0.0148	118.4	211.0 (3)	0.136	141.7	45.9
O-∗-Te/**1j**$^{\bullet+}$	0.0473	0.0106	−0.0092	−1.302	0.0141	130.9	187.7 (3)	0.127	151.1	4.4
				Dicationic Species						
S-∗-S/**1a**$^{2+}$	0.1351	−0.0133	−0.0708	−2.601	0.0720	190.6	425.6 (8)	0.551	198.1	0.5
S-∗-Se/**1b**$^{2+}$	0.1155	−0.0078	−0.0558	−2.387	0.0563	187.9	377.0 (8)	0.565	192.0	0.8
S-∗-Te/**1c**$^{2+}$	0.0923	−0.0013	−0.0419	−2.067	0.0420	181.8	355.2 (8)	0.456	171.9	22.9
Se-∗-Se/**1d**$^{2+}$	0.1032	−0.0070	−0.0471	−2.427	0.0476	188.5	263.3 (5)	0.238	192.3	0.6
Se-∗-Te/**1e**$^{2+}$	0.0867	−0.0046	−0.0390	−2.313	0.0392	186.8	249.4 (6)	0.275	184.9	24.7
Te-∗-Te/**1f**$^{2+}$	0.0760	−0.0054	−0.0313	−2.530	0.0318	189.8	196.7 (4)	0.781	193.4	1.1
O-∗-O/**1g**$^{2+}$	0.0325	0.0158	0.0041	−0.850	0.0163	75.4	252.1 (3)	0.161	74.1	20.8
O-∗-S/**1h**$^{2+}$	0.1765	−0.0240	−0.1774	−2.370	0.1790	187.7	586.3 (10)	1.274	172.3	2.3
O-∗-Se/**1i**$^{2+}$	0.1407	0.0171	−0.0877	−1.720	0.0894	169.0	518.9 (9)	0.801	166.4	5.6
O-∗-Te/**1j**$^{2+}$	0.1079	0.0416	−0.0368	−1.307	0.0555	131.5	506.6 (9)	0.754	110.4	1.2

[a]For BSS-B: The 6-311+G(3df) basis set for O, S, and Se and that of the (7433111/743111/7411/2 + 1s1p1d1f) type for Te with the 6-311+G(d,p) basis set for C and H. [b]$c = \hbar^2/8m$. [c]$k_b(\mathbf{r}_c) = V_b(\mathbf{r}_c)/G_b(\mathbf{r}_c)$. [d]Corresponding to the E−E′ bond in question. [e]BCP being not detected.

$(=V_b(\mathbf{r}_c)/G_b(\mathbf{r}_c))$ of E-∗-E′ at BCP[67] in **1a**−**1j**, **1a**$^{\bullet+}$−**1j**$^{\bullet+}$, and **1a**$^{2+}$−**1j**$^{2+}$. Table 2 collects the values, although BCP of S-∗-Se is not detected for **1b**, maybe due to the disadvantageous steric reason. Figure 13 shows the plots of $H_b(\mathbf{r}_c)$ versus $H_b(\mathbf{r}_c) - V_b(\mathbf{r}_c)/2$ for the data of the fully optimized structures, together with those of the perturbed structures around the fully optimized ones. Figure 13a−c corresponds to the plots for **1a**−**1j**, **1a**$^{\bullet+}$−**1j**$^{\bullet+}$, and **1a**$^{2+}$−**1j**$^{2+}$, respectively. Data of a plot for each E-∗-E′ interaction are connected by a regression curve, assuming the cubic function shown in eq 10, for **1a**−**1j**, **1a**$^{\bullet+}$−**1j**$^{\bullet+}$, and **1a**$^{2+}$−**1j**$^{2+}$. However, data of some plots are described as the line graph type if data cannot be connected as one-valued functions, such as those of **1h**$^{2+}$ (O-∗-S).[68] Figure 13d shows the similar plots for **2a**−**2j**, for convenience of comparison. Plots for **1a**$^{2+}$−**1j**$^{2+}$ in Figure 13c are very similar to those for **2a**−**2j** in Figure 13d, except for the plot for **1g**$^{2+}$ (O-∗-O) versus that **2g** (O-∗-O).

DOI: 10.1021/acs.joc.5b01794
J. Org. Chem. 2015, 80, 11963−11976

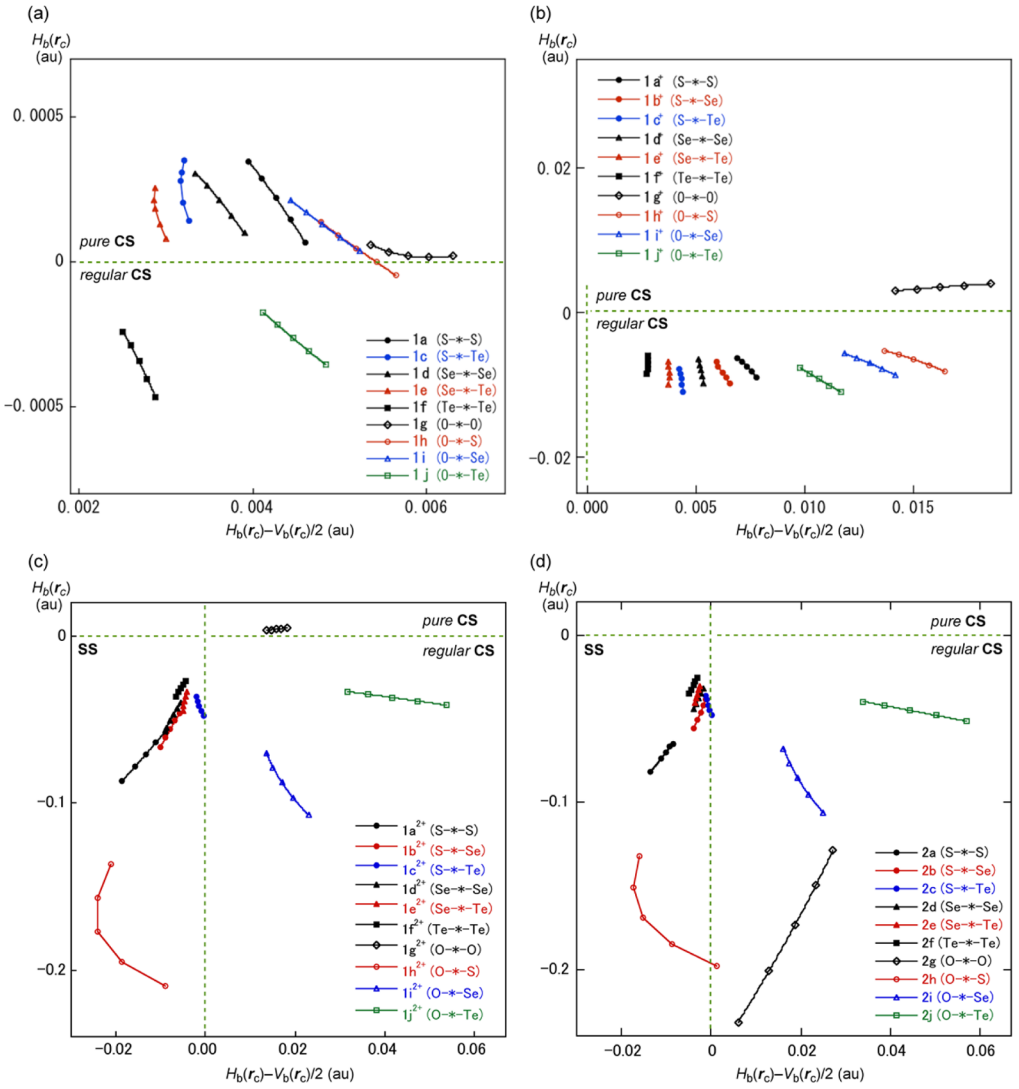

Figure 13. Plots of $H_b(\mathbf{r}_c)$ versus $H_b(\mathbf{r}_c) - V_b(\mathbf{r}_c)/2$ for **1** (a), $\mathbf{1}^{\bullet+}$ (b), and $\mathbf{1}^{2+}$ (c), together with **2** (d).

As shown in Figure 13a, all data of **1a**−**1j** appear in the pure CS region ($H_b(\mathbf{r}_c) - V_b(\mathbf{r}_c)/2 > 0$ and $H_b(\mathbf{r}_c) > 0$), except for those of **1f** (Te-∗-Te) and **1j** (O-∗-Te), which appear in the regular CS region ($H_b(\mathbf{r}_c) - V_b(\mathbf{r}_c)/2 > 0$ and $H_b(\mathbf{r}_c) < 0$). In the case of $\mathbf{1a}^{\bullet+}$−$\mathbf{1j}^{\bullet+}$, all data appear in the regular CS region, except for those of $\mathbf{1g}^{\bullet+}$ (O-∗-O), which appear in the pure CS region (Figure 13b). On the other hand, data of $\mathbf{1a}^{2+}$−$\mathbf{1f}^{2+}$ and $\mathbf{1h}^{2+}$ (O-∗-S) appear in the SS region ($H_b(\mathbf{r}_c) - V_b(\mathbf{r}_c)/2 < 0$ and $H_b(\mathbf{r}_c) < 0$), whereas those of $\mathbf{1i}^{2+}$ (O-∗-Se) and $\mathbf{1j}^{2+}$ (O-∗-Te) drop in the regular CS region with those of $\mathbf{1g}^{2+}$ (O-∗-O) in the pure CS region.

QTAIM-DFA parameters of (R, θ) and (θ_p, κ_p) are obtained through analysis of the plots for **1a**−**1j**, $\mathbf{1a}^{\bullet+}$−$\mathbf{1j}^{\bullet+}$, and $\mathbf{1a}^{2+}$−$\mathbf{1j}^{2+}$, according to eqs 3−6. The (R, θ) and (θ_p, κ_p) values are collected in Table 2, together with the frequencies (ν's) and force constants (k_f's) corresponding to the E-∗-E′ interactions in question.

The behavior of E-∗-E′ in **1a**−**1j**, $\mathbf{1a}^{\bullet+}$−$\mathbf{1j}^{\bullet+}$, and $\mathbf{1a}^{2+}$−$\mathbf{1j}^{2+}$ is examined, next, by employing the R, θ, and θ_p values, mainly, together with those in Scheme 2, as a reference.

Nature of E-∗-E′ in 1, $1^{\bullet+}$, and 1^{2+}, Elucidated with (R, θ) and (θ_p, κ_p). It is instructive to survey the criteria, before a detailed discussion of the nature of E-∗-E′. Scheme 2 tells us that $\theta < 180°$ for the CS interactions, whereas $\theta > 180°$ for the SS interactions. The CS and SS interactions correspond to $H_b(\mathbf{r}_c) - V_b(\mathbf{r}_c)/2 > 0$ and $H_b(\mathbf{r}_c) - V_b(\mathbf{r}_c)/2 < 0$, respectively. The CS interactions are divided into pure CS and regular CS interactions for $45° < \theta < 90°$ and $90° < \theta < 180°$, respectively, which correspond to $H_b(\mathbf{r}_c) > 0$ and $H_b(\mathbf{r}_c) < 0$, respectively, with $H_b(\mathbf{r}_c) - V_b(\mathbf{r}_c)/2 > 0$. The θ_p value will play an important role to determine the characters of the interactions. In the pure CS region of $45° < \theta < 90°$, the character of interactions will be the vdW type for $45° < \theta_p < 90°$ or the typical HB type with no covalency for $90° < \theta_p < 125°$, although θ_p of 125° tentatively corresponds to $\theta = 90°$. The CT interactions will appear in the regular CS region of $90° < \theta < 180°$. Interactions of the CT-MC and CT-TBP types will appear in the ranges $150° \leq \theta_p < 180°$ ($115° \leq \theta < 150°$) and $180° \leq \theta_p < 190°$ ($150° \leq \theta < 180°$), respectively. Typical HB interactions with covalency will appear in the region of $125° \leq \theta_p < 150°$ ($90° \leq \theta < 115°$). CT will contribute to typical HBs in this region. The value of R classifies SS, further. Classical chemical bonds of SS are strong when $R > 0.15$ au, but they will be weak if $R < 0.15$ au.

Table 3 collects the characters of the E-∗-E′ interactions in **1a**−**1j**, $\mathbf{1a}^{\bullet+}$−$\mathbf{1j}^{\bullet+}$, and $\mathbf{1a}^{2+}$−$\mathbf{1j}^{2+}$, determined using the R, θ, and θ_p values, together with **2a**−**2j**, for convenience of

DOI: 10.1021/acs.joc.5b01794
J. Org. Chem. 2015, 80, 11963−11976

Table 3. Classification and Characterization of E···E′ in the Neutral, Radical Cationic, and Dicationic Forms in *cyclo*-1,5-E($CH_2CH_2CH_2$)$_2$E′ (1), Together with the Neutral forms of *cyclo*-1,2-E ($CH_2CH_2CH_2$)E′ (2), Evaluated with NIV at the MP2 Level[a]

interaction (E-∗-E′)	R (au)	θ (deg)	θ_p (deg)	classification/character	interaction (E-∗-E′)	R (au)	θ (deg)	θ_p (deg)	classification/character
Neutral Species									
S-∗-S/**1a**	0.004	87.0	113.2	*p*-CS/*t*-HB	O-∗-O/**1g**	0.006	89.8	92.6	*p*-CS/*t*-HB
S-∗-Se/**1b**	*b*	*b*	*b*	*b*	O-∗-S/**1h**	0.005	89.5	101.8	*p*-CS/*t*-HB
S-∗-Te/**1c**	0.003	84.9	170.8	*p*-CS/*t*-HB	O-∗-Se/**1i**	0.005	88.5	102.5	*p*-CS/*t*-HB
Se-∗-Se/**1d**	0.004	86.6	110.3	*p*-CS/*t*-HB	O-∗-Te/**1j**	0.005	93.4	104.1	*r*-CS/*t*-HB
Se-∗-Te/**1e**	0.003	86.4	142.1	*p*-CS/*t*-HB					
Te-∗-Te/**1f**	0.003	97.3	121.0	*r*-CS/*t*-HB					
Radical Cationic Species									
S-∗-S/**1a**$^{\bullet+}$	0.011	135.6	162.3	*r*-CS/CT-MC	O-∗-O/**1g**$^{\bullet+}$	0.017	77.8	77.6	*p*-CS/vdW
S-∗-Se/**1b**$^{\bullet+}$	0.010	143.1	165.8	*r*-CS/CT-MC	O-∗-S/**1h**$^{\bullet+}$	0.016	113.4	135.6	*r*-CS/CT-MC
S-∗-Te/**1c**$^{\bullet+}$	0.010	154.9	177.3	*r*-CS/CT-MC	O-∗-Se/**1i**$^{\bullet+}$	0.015	118.4	141.7	*r*-CS/CT-MC
Se-∗-Se/**1d**$^{\bullet+}$	0.010	146.9	175.7	*r*-CS/CT-MC	O-∗-Te/**1j**$^{\bullet+}$	0.014	130.9	151.1	*r*-CS/CT-MC
Se-∗-Te/**1e**$^{\bullet+}$	0.009	155.5	179.8	*r*-CS/CT-MC					
Te-∗-Te/**1f**$^{\bullet+}$	0.008	158.8	181.6	*r*-CS/CT-TBP					
Dicationic Species									
S-∗-S/**1a**$^{2+}$	0.072	190.6	198.1	SS/Cov-w	O-∗-O/**1g**$^{2+}$	0.016	75.4	74.1	*p*-CS/vdW
S-∗-Se/**1b**$^{2+}$	0.056	187.9	192.0	SS/Cov-w	O-∗-S/**1h**$^{2+}$	0.179	187.7	172.3	SS/CT-MC
S-∗-Te/**1c**$^{2+}$	0.042	181.8	171.9	SS/CT-MC	O-∗-Se/**1i**$^{2+}$	0.089	169.0	166.4	*r*-CS/CT-MC
Se-∗-Se/**1d**$^{2+}$	0.048	188.5	192.3	SS/Cov-w	O-∗-Te/**1j**$^{2+}$	0.056	131.5	110.4	*r*-CS/*t*-HB
Se-∗-Te/**1e**$^{2+}$	0.039	186.8	184.9	SS/CT-TBP					
Te-∗-Te/**1f**$^{2+}$	0.032	189.8	193.4	SS/Cov-w					
Neutral Species									
S-∗-S/**2a**	0.068	190.2	198.1	SS/Cov-w	O-∗-O/**2g**	0.175	173.9	191.5	*p*-CS/CT-TBP
S-∗-Se/**2b**	0.047	183.5	189.8	SS/CT-TBP	O-∗-S/**2h**	0.170	185.1	165.9	SS/CT-MC
S-∗-Te/**2c**	0.042	174.8	165.5	*r*-CS/CT-MC	O-∗-Se/**2i**	0.088	167.3	167.8	*r*-CS/CT-MC
Se-∗-Se/**2d**	0.038	184.1	188.9	SS/CT-TBP	O-∗-Te/**2j**	0.063	135.4	117.0	*r*-CS/*t*-HB
Se-∗-Te/**2e**	0.036	182.3	180.3	SS/CT-TBP					
Te-∗-Te/**2f**	0.030	187.1	190.2	SS/Cov-w					

[a]Data from Table 2. [b]BCP being not detected.

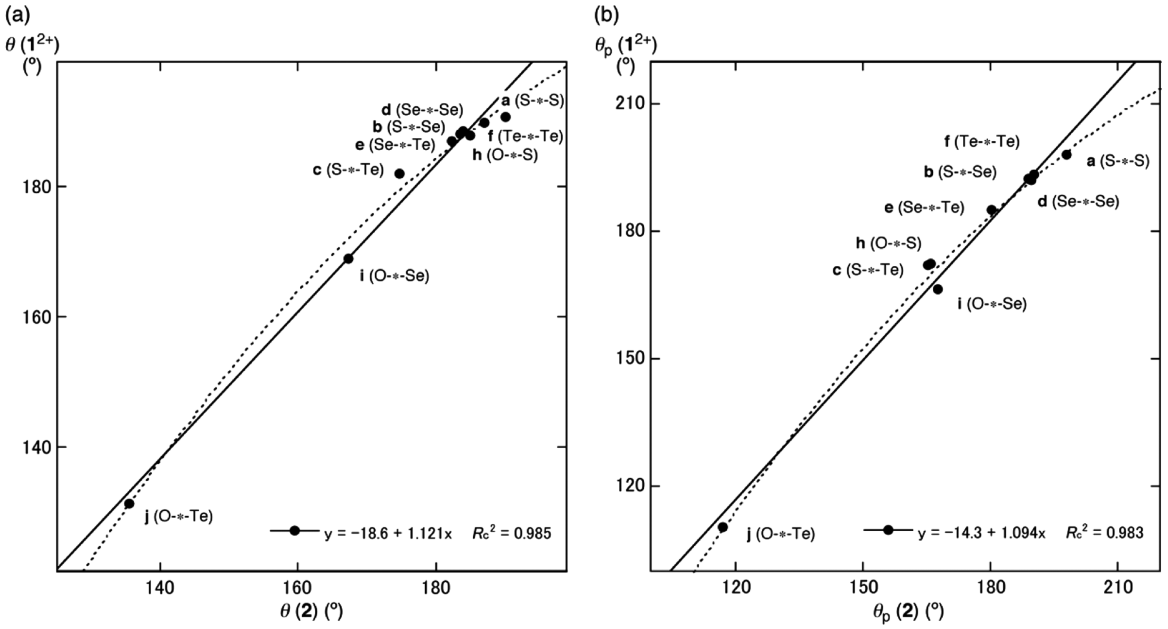

Figure 14. Plot of θ for **1a**$^{2+}$−**1j**$^{2+}$ versus those for **2a**−**2f** (a) and that of θ_p for **1a**$^{2+}$−**1j**$^{2+}$ versus those for **2a**−**2f** (b). Data for **1g**$^{2+}$ and **2g** are not shown in the plots.

comparison. The interactions become stronger in the order of **1a**−**1j** < **1a**$^{\bullet+}$−**1j**$^{\bullet+}$ < **1a**$^{2+}$−**1j**$^{2+}$, if the same E-∗-E′ are compared, except for O-∗-O. The O-∗-O interaction seems weaker in the order of **1g** (O-∗-O) > **1g**$^{\bullet+}$ (O-∗-O) > **1g**$^{2+}$ (O-∗-O), judging from the θ and θ_p values. The trend is inverse, relative to the cases of other E-∗-E′ interactions in Table 3. All

DOI: 10.1021/acs.joc.5b01794
J. Org. Chem. 2015, 80, 11963−11976

E-∗-E′ in **1a**−**1j** are characterized as typical HB nature with no covalency appearing in the pure CS region, except for Te-∗-Te in **1f** and O-∗-Te in **1j**, which are characterized as typical HB nature with covalency appearing in the regular CS-region. BCP is not detected for S-∗-Se in **1b**. Similarly, E-∗-E′ in $\mathbf{1a}^{\bullet+}$−$\mathbf{1j}^{\bullet+}$ are all characterized as CT-MC appearing at the regular CS region, except for Te-∗-Te in $\mathbf{1f}^{\bullet+}$ and O-∗-O in $\mathbf{1g}^{\bullet+}$, which are characterized as CT-TBP appearing at the regular CS region and the vdW nature appearing at the pure CS region, respectively.

In the case of E-∗-E′ in $\mathbf{1a}^{2+}$−$\mathbf{1f}^{2+}$, they are all classified by the SS interactions (θ > 180°) and characterized to have the Cov-w nature (θ_p > 180°: R < 0.15 au), except for S-∗-Te in $\mathbf{1c}^{2+}$ (θ_p = 172°) and Se-∗-Te in $\mathbf{1e}^{2+}$ (θ_p = 185°), which should be characterized to have the CT-MC and CT-TBP nature, respectively (appearing in the SS region). On the other hand, the behavior of O-∗-E′ in $\mathbf{1g}^{2+}$−$\mathbf{1j}^{2+}$ seems somewhat complex. The interactions of O-∗-O in $\mathbf{1g}^{2+}$, O-∗-S in $\mathbf{1h}^{2+}$, O-∗-Se in $\mathbf{1i}^{2+}$, and O-∗-Te in $\mathbf{1j}^{2+}$ are classified and characterized as (pure CS; vdW), (SS; CT-MC), (regular CS; CT-MC), and (regular CS; typical HB with covalent nature), respectively. Indeed, S-∗-Te in $\mathbf{1c}^{2+}$ and O-∗-S in $\mathbf{1h}^{2+}$ are characterized as CT-MC with their θ_p values, but the interactions should be characterized as Cov-w and Cov-s, respectively, if θ values are mainly considered. The dynamic behavior of S-∗-Te in $\mathbf{1c}^{2+}$ and O-∗-S in $\mathbf{1h}^{2+}$ seems very complex, which should be clarified further.

The (R, θ, θ_p) values for O-∗-S in $\mathbf{1h}^{2+}$ are (0.179 au, 187.7°, 172.3°). The (R, θ) values seem to satisfy the requirements for O-∗-S in $\mathbf{1h}^{2+}$ to be classified by Cov-s, of which data appear in the SS region. However, the θ_p value of 172.3° corresponds to the CT-MC region for O-∗-S in $\mathbf{1h}^{2+}$. The O-∗-S in $\mathbf{1h}^{2+}$ is characterized by CT-MC as shown in Table 3, as are other cases of interactions. However, the results strongly suggest that the O-∗-S interactions must be more complex than those clarified in this work. This discrepancy must be the reflection of the fact that θ_p is less than θ for O-∗-S in $\mathbf{1h}^{2+}$, although θ_p are larger than θ for usual cases. The complex behavior in O-∗-S in $\mathbf{1h}^{2+}$ (and **2h**) can be confirmed in the plot shown in Figure 13c (and Figure 13d). The reason and/or mechanisms should also be elucidated further.

As mentiond above, the behavior of E−E′ in $\mathbf{1a}^{2+}$−$\mathbf{1j}^{2+}$ is very similar to that in **2a**−**2f**, respectively, except for $\mathbf{1g}^{2+}$ (O-∗-O)/**2g** (O-∗-O). Figure 14a,b shows the plot of θ and θ_p for $\mathbf{1a}^{2+}$−$\mathbf{1j}^{2+}$ versus those for **2a**−**2f**, respectively. The plot in Figure 14a gives a very good correlation, which is shown in the figure. The θ values of $\mathbf{1a}^{2+}$−$\mathbf{1j}^{2+}$ are linearly well-correlated with those of **2a**−**2f**, although the correlation would be better analyzed as parabolic ($y = -202.4 + 3.426x - 0.007x^2$: R_c^2 = 0.993, without data for $\mathbf{1g}^{2+}$/**2g**). Similarly, the plot for θ_p in Figure 14b shows a very good correlation, which is given in the figure. The correlation would also be better analyzed as parabolic ($y = -110.4 + 2.356x - 0.004x^2$: R_c^2 = 0.992, without data for $\mathbf{1g}^{2+}$/**2g**). The θ and θ_p values for $\mathbf{1a}^{2+}$−$\mathbf{1j}^{2+}$ are demonstrated to be linearly correlated to those in **2a**−**2j**, respectively, as a whole. The R values in (R, θ) for $\mathbf{1a}^{2+}$−$\mathbf{1j}^{2+}$ are also plotted versus those of **2a**−**2f**, which is shown in Figure S7 of the Supporting Information. The plot gives a very good correlation ($y = 1.027x + 0.0017$; R_c^2 = 0.986), where data for **g** (O-∗-O) are neglected from the correlation, again. The results clarify well the similarities in the behvior of E−E′ between $\mathbf{1a}^{2+}$−$\mathbf{1j}^{2+}$ and **2a**−**2f**, except for $\mathbf{1g}^{2+}$/**2g**. The E−E′ interactions in $\mathbf{1}^{2+}$ and **2** can be described by σ(2c−2e), which must be the main reason for the similarity, although n_p(E) and n_p(E′) in **2** are replaced by E−C σ(2c−2e) and E′−C′ σ(2c−2e) in $\mathbf{1}^{2+}$, respectively.

The behavior of E−E′ in **1**, $\mathbf{1}^{\bullet+}$, and $\mathbf{1}^{2+}$ is well-clarified by QTAIM-DFA, and the similarities in E−E′ between $\mathbf{1}^{2+}$ and **2** are confirmed by the QTAIM-DFA parameters, except for O-∗-O.

CONCLUSION

The nature of the E−E and E···E′ interactions in neutral, radical cationic, and dicationic forms of 1,5-*cyclo*-E($CH_2CH_2CH_2$)$_2$E′ (**1**) ((E, E′) = **a** (S, S), **b** (S, Se), **c** (S, Te), **d** (Se, Se), **e** (Se, Te), **f** (Te, Te), **g** (O, O), **h** (O, S), **i** (O, Se), and **j** (O, Te)) (**1a**−**1j**, $\mathbf{1a}^{\bullet+}$−$\mathbf{1j}^{\bullet+}$, and $\mathbf{1a}^{2+}$−$\mathbf{1j}^{2+}$, respectively) are elucidated by applying QTAIM-DFA. Structures are optimized with BSS-B at the MP2 level for **1a**−**1j**, $\mathbf{1a}^{\bullet+}$−$\mathbf{1j}^{\bullet+}$, and $\mathbf{1a}^{2+}$−$\mathbf{1j}^{2+}$ of the chair-boat (**CB**) forms. QTAIM functions are calculated with the same basis set system at the MP2 level. The molecular graphs, contour plots, negative Laplacians, and trajectory plots are drawn for the species, which depicts the basis nature of E-∗-E′ in the species. $H_b(\mathbf{r}_c)$ are plotted versus $H_b(\mathbf{r}_c) - V_b(\mathbf{r}_c)/2$ for the data of E-∗-E′ at BCPs of fully optimized structures and perturbed structures around the fully optimized ones. The plots are analyzed according to the definitions in QTAIM-DFA. Plots for the data of fully optimized structures are analyzed by the polar coordinate (R, θ) representation. The (θ_p, κ_p) parameters are derived from those containing the perturbed structures: θ_p corresponds to the tangent line of each plot, and κ_p is the curvature. While (R, θ) correspond to the static nature, (θ_p, κ_p) represent the dynamic nature of interactions.

QTAIM parameters of R, θ, and θ_p are mainly employed to clarify the nature of E-∗-E′ in **1a**−**1j**, $\mathbf{1a}^{\bullet+}$−$\mathbf{1j}^{\bullet+}$, and $\mathbf{1a}^{2+}$−$\mathbf{1j}^{2+}$, using those of the standard values as a reference. Each E-∗-E′ becomes stronger in the order **1a**−**1j** < $\mathbf{1a}^{\bullet+}$−$\mathbf{1j}^{\bullet+}$ < $\mathbf{1a}^{2+}$−$\mathbf{1j}^{2+}$, if the same E-∗-E′ is compared, except for O-∗-O. The O-∗-O interactions become weakened in the order **1g** > $\mathbf{1g}^{\bullet+}$ > $\mathbf{1g}^{2+}$, judging from the θ and θ_p values. All E-∗-E′ in **1a**−**1j** are characterized as typical HB with no covalency appearing in the pure CS region, except for Te-∗-Te in **1f** and O-∗-Te in **1j**, which are characterized as the typical-HB with covalency appearing in the regular CS region. BCP is not detected for S-∗-Se in **1b**. Similarly, all E-∗-E′ in $\mathbf{1a}^{\bullet+}$−$\mathbf{1j}^{\bullet+}$ characterized as CT-TBP appeared in the regular CS region, except for Te-∗-Te in $\mathbf{1f}^{\bullet+}$ and O-∗-O in $\mathbf{1g}^{\bullet+}$, which are characterized as CT-TBP appearing in the regular CS region and the vdW type appearing in the pure CS region, respectively. The E-∗-E′ interactions in $\mathbf{1a}^{2+}$−$\mathbf{1f}^{2+}$ are all classified by SS (θ > 180°) and characterized to have the Cov-w nature (θ_p > 180°: R < 0.15 au), except for S-∗-Te in $\mathbf{1c}^{2+}$ (θ_p = 172°) and Se-∗-Te in $\mathbf{1e}^{2+}$ (θ_p = 185°), which should be characterized to have the CT-MC and CT-TBP nature, respectively (appeared in the SS region). On the other hand, the interactions of O-∗-O in $\mathbf{1g}^{2+}$, O-∗-S in $\mathbf{1h}^{2+}$, O-∗-Se in $\mathbf{1i}^{2+}$, and O-∗-Te in $\mathbf{1j}^{2+}$ are classified and characterized as (pure CS; vdW), (SS; CT-MC), (regular CS; CT-MC), and (regular CS; typical HB with covalent nature), respectively. The (R, θ, θ_p) values for O-∗-S in $\mathbf{1h}^{2+}$ are (0.179 au, 187.7°, 172.3°). The (R, θ) values satisfy the requirements for O-∗-S in $\mathbf{1h}^{2+}$ to have the Cov-s nature appeared in the SS region. However, it should be classified to have the CT-MC nature, if θ_p of 172.3° is mainly considered. The O-∗-S interaction must be analyzed carefully. The behaviors of E−E′ in $\mathbf{1a}^{2+}$−$\mathbf{1j}^{2+}$ are very similar to those in **2a**−**2j**, respectively, except for $\mathbf{1g}^{2+}$/**2g** (O-∗-O). The E−E′ in $\mathbf{1}^{2+}$ and **2** can be

DOI: 10.1021/acs.joc.5b01794
J. Org. Chem. 2015, 80, 11963−11976

described by E−E′ σ(2c−2e), which must be the main reason for the similarity, although n_p(E) and n_p(E′) in **2** are replaced by E−C σ(2c−2e) and E′−C′ σ(2c−2e) in $\mathbf{1}^{2+}$, respectively. Indeed, the nature of E−E′ is well-clarified with QTAIM-DFA, but some seem in the dark, which should be elucidated further.

■ ASSOCIATED CONTENT

Supporting Information

The Supporting Information is available free of charge on the ACS Publications website at DOI: 10.1021/acs.joc.5b01794.

Computational data (Tables S1−S4 and Figures S1−S7), the fullly optimized structures given by Cartesian coordinates, together with total energiess, and complete ref 51 (PDF)

■ AUTHOR INFORMATION

Corresponding Authors

*E-mail: hayashi3@sys.wakayama-u.ac.jp.

*E-mail: nakanisi@sys.wakayama-u.ac.jp. Phone: +81 73 457 8252. Fax: +81 73 457 8253.

Notes

The authors declare no competing financial interest.

■ ACKNOWLEDGMENTS

This work was partially supported by a Grant-in-Aid for Scientific Research (No. 26410050) from the Ministry of Education, Culture, Sports, Science and Technology, Japan. The support of the Wakayama University Original Research Support Project Grant and the Wakayama University Graduate School Project Research Grant is also acknowledged.

■ REFERENCES

(1) (a) *Organic Selenium Compounds: Their Chemistry and Biology*; Klayman, D. L., Günther, W. H. H., Eds.; Wiley: New York, 1973. (b) *The Chemistry of Organic Selenium and Tellurium Compounds*; Patai, S., Rappoport, Z., Eds.; John-Wiley and Sons: New York, 1986, Vols. *1* and *2*. (c) *Organic Selenium Chemistry*; Liotta, D., Ed.; Wiley-Interscience: New York, 1987. (d) *Organoselenium Chemistry, A Practical Approach*; Back, T. G., Ed.; Oxford University Press: Oxford, 1999. (e) *Organoselenium Chemistry, Modern Developments in Organic Synthesis, Topics in Current Chemistry*; Wirth, T., Ed.; Springer: Berlin, 2000.

(2) *Chemistry of Hypervalent Compounds*; Akiba, K.-y., Ed.; Wiley-VCH: New York, 1999.

(3) (a) Nakanishi, W. In *Handbook of Chalcogen Chemistry: New Perspectives in Sulfur, Selenium and Tellurium*; Devillanova, F. A., Ed.; Royal Society of Chemistry: Cambridge, U.K., 2006, Chapter 10.3, pp 644−668. (b) Nakanishi, W.; Hayashi, S. In *Handbook of Chalcogen Chemistry: New Perspectives in Sulfur, Selenium and Tellurium*, 2nd ed.; Devillanova, F. A., du Mont, W.-W., Eds.; Royal Society of Chemistry: Cambridge, U.K., 2013; Vol. *2*, Chapter 12.3, pp 335−372.

(4) Mukherjee, A. J.; Zade, S. S.; Singh, H. B.; Sunoj, R. B. *Chem. Rev.* **2010**, *110*, 4357−4416.

(5) (a) Morihashi, K.; Kushihara, S.; Inadomi, Y.; Kikuchi, O. *J. Mol. Struct.: THEOCHEM* **1997**, *418*, 171−178. (b) Mueller, B.; Takaluoma, T. T.; Laitinen, R. S.; Seppelt, K. *Eur. J. Inorg. Chem.* **2011**, *2011*, 4970−4977. (c) Mueller, B.; Poleschner, H.; Seppelt, K. *Dalton Trans.* **2008**, 4424−4427. (d) Wakamiya, A.; Nishinaga, T.; Komatsu, K. *J. Am. Chem. Soc.* **2002**, *124*, 15038−15050. (e) Mundt, O.; Becker, G.; Baumgarten, J.; Riffel, H.; Simon, A. *Z. Anorg. Allg. Chem.* **2006**, *632*, 1687−1709.

(6) One of reviewers recommended that we use "hard-shell" instead of "shared-shell" for E−E′. However, "shared-shell" is used in this paper.

(7) Bhuyan, B. J.; Lamani, D. S.; Mugesh, G.; Wirth, T. In *Handbook of Chalcogen Chemistry: New Perspectives in Sulfur, Selenium and Tellurium*, 2nd ed.; Devillanova, F. A., du Mont, W.-W., Eds.; Royal Society of Chemistry: Cambridge, U.K., 2013; Vol. *2*, Chapter 10.2, pp 25−46.

(8) Jakka, S. R.; Mugesh, G. In *Handbook of Chalcogen Chemistry: New Perspectives in Sulfur, Selenium and Tellurium*, 2nd ed.; Devillanova, F. A., du Mont, W.-W., Eds.; Royal Society of Chemistry: Cambridge, U.K., 2013; Vol. *2*, Chapter 10.3, pp 46−65.

(9) *The Chemistry of Organic Selenium and Tellurium Compounds*; Patai, S., Rappoport, Z., Eds.; Wiley: New York, 1986; *Vol. 1*, Chapter 6.

(10) *The Chemistry of Organic Selenium and Tellurium Compounds*; Rappoport, Z., Ed.; Wiley: New York, 2013; Vol. *4*, Chapters 13−16.

(11) (a) Panda, A.; Mugesh, G.; Singh, H. B.; Butcher, R. *Organometallics* **1999**, *18*, 1986−1993. (b) Kulcsar, M.; Beleaga, A.; Silvestru, C.; Nicolescu, A.; Deleanu, C.; Todasca, C.; Silvestru, A. *Dalton Trans.* **2007**, 2187−2196. (c) Beleaga, A.; Kulcsar, M.; Deleanu, C.; Nicolescu, A.; Silvestru, C.; Silvestru, A. *J. Organomet. Chem.* **2009**, *694*, 1308−1316.

(12) Nakanishi, W.; Hayashi, S.; Morinaka, S.; Sasamori, T.; Tokitoh, N. *New J. Chem.* **2008**, *32*, 1881−1889.

(13) (a) Iwasaki, F.; Toyoda, N.; Akaishi, R.; Fujihara, H.; Furukawat, N. *Bull. Chem. Soc. Jpn.* **1988**, *61*, 2563−2567. (b) Fujihara, H.; Kawada, A.; Furukawa, N. *J. Org. Chem.* **1987**, *52*, 4254−4257.

(14) (a) Iwasaki, F.; Morimoto, M.; Yasui, M.; Akaishi, R.; Fujihara, H.; Furukawa, N. *Acta Crystallogr., Sect. C: Cryst. Struct. Commun.* **1991**, *C47*, 1463−1466. (b) Fujihara, H.; Furukawa, N. *Phosphorus, Sulfur Silicon Rel. Elem.* **1992**, *67*, 131−134.

(15) (a) Fujihara, H.; Akaishi, R.; Erata, T.; Furukawa, N. *J. Chem. Soc., Chem. Commun.* **1989**, 1789−1790. (b) Fujihara, H.; Akaishi, R.; Furukawa, N. *Tetrahedron* **1993**, *49*, 1605−1618.

(16) Fujihara, H.; Akaishi, R.; Nakamura, A.; Furukawa, N. *Tetrahedron Lett.* **1990**, *31*, 6375−6378.

(17) Fujihara, H.; Yabe, M.; Chiu, J.-J.; Furukawa, N. *Tetrahedron Lett.* **1991**, *32*, 4345−4348.

(18) Fujihara, H.; Ninoi, T.; Akaishi, R.; Erata, T.; Furukawa, N. *Tetrahedron Lett.* **1991**, *32*, 4537−4540.

(19) Fujihara, H.; Takuguchi, Y.; Ninoi, T.; Erata, T.; Furukawa, N. *J. Chem. Soc., Perkin Trans. 1* **1992**, 2583−2584.

(20) Fujihara, H.; Furukawa, N. *J. Mol. Struct.: THEOCHEM* **1989**, *186*, 261−272.

(21) Nakayama, N.; Takahashi, O.; Kikuchi, O.; Furukawa, N. *Heteroat. Chem.* **2000**, *11*, 31−41.

(22) Nakayama, N.; Takahashi, O.; Kikuchi, O.; Furukawa, N. *J. Mol. Struct.: THEOCHEM* **2001**, *542*, 215−226.

(23) (a) Block, E.; Dikarev, E. V.; Glass, R. S.; Jin, J.; Li, B.; Li, X.; Zhang, S.-Z. *J. Am. Chem. Soc.* **2006**, *128*, 14949−14961. (b) Block, E.; Glass, R. S.; Dikarev, E. V.; Gruhn, N. E.; Jin, J.; Li, B.; Lorance, E.; Zakai, U. I.; Zhang, S. Z. *Heteroat. Chem.* **2007**, *18*, 509−515. (c) Liao, C.; Zhang, S.-Z.; Block, E.; Clennan, E. L. *J. Org. Chem.* **2008**, *73*, 8587−8590.

(24) (a) Glass, R. S.; Block, E.; Lorance, E.; Zakai, U. I.; Gruhn, N. E.; Jin, J.; Zhang, S.-Z. *J. Am. Chem. Soc.* **2006**, *128*, 12685−12692. (b) Glass, R. S.; Block, E.; Gruhn, N. E.; Jin, J.; Lorance, E.; Zakai, U. I.; Zhang, S.-Z. *J. Org. Chem.* **2007**, *72*, 8290−8297.

(25) (a) Glass, R. S.; Adamowicz, L.; Broeker, J. L. *J. Am. Chem. Soc.* **1991**, *113*, 1065−1072. (b) Glass, R. S.; Andruski, S. W.; Broeker, J. L.; Firouzabadi, H.; Steffen, L. K.; Wilson, G. S. *J. Am. Chem. Soc.* **1989**, *111*, 4036−4045.

(26) Evans, D. H.; Gruhn, N. E.; Jin, J.; Li, B.; Lorance, E.; Okumura, N.; Macias-Ruvalcaba, N. A.; Zakai, U. I.; Zhang, S.-Z.; Block, E.; Glass, R. S. *J. Org. Chem.* **2010**, *75*, 1997−2009.

(27) Stowasser, R.; Glass, R. S.; Hoffmann, R. *J. Chem. Soc., Perkin Trans. 2* **1999**, 1559−1561.

(28) The electronegativity proposed by Allred-Rochow was employed to discuss the structure of the adducts. See: (a) Allred, A. L.; Rochow, E. G. J. *J. Inorg. Nucl. Chem.* **1958**, *5*, 264−268. (b) Allred, A. L.; Rochow, E. G. J. *J. Inorg. Nucl. Chem.* **1958**, *5*, 269−288.

DOI: 10.1021/acs.joc.5b01794
J. Org. Chem. 2015, 80, 11963−11976

(29) Musker, W. K.; Wolford, T. L. *J. Am. Chem. Soc.* **1976**, *98*, 3055−3056.
(30) (a) Musker, W. K.; Wolford, T. L.; Roush, P. D. *J. Am. Chem. Soc.* **1978**, *100*, 6416−6421. (b) Musker, W. K. *Acc. Chem. Res.* **1980**, *13*, 200−206.
(31) (a) Asmus, K.-D. *Acc. Chem. Res.* **1979**, *12*, 436−442. (b) Maity, D. K. *J. Am. Chem. Soc.* **2002**, *124*, 8321−8328. See also ref 22.
(32) (a) *Atoms in Molecules. A Quantum Theory*; Bader, R. F. W., Ed.; Oxford University Press: Oxford, U.K., 1990. (b) Matta, C. F.; Boyd, R. J. In *The Quantum Theory of Atoms in Molecules: From Solid State to DNA and Drug Design*; Matta, C. F., Boyd, R. J., Eds.; WILEY-VCH: Weinheim, Germany, 2007; Chapter 1.
(33) (a) Bader, R. F. W.; Slee, T. S.; Cremer, D.; Kraka, E. *J. Am. Chem. Soc.* **1983**, *105*, 5061−5068. (b) Bader, R. F. W. *Chem. Rev.* **1991**, *91*, 893−928. (c) Bader, R. F. W. *J. Phys. Chem. A* **1998**, *102*, 7314−7323. (d) Biegler-König, F.; Bader, R. F. W.; Tang, T. H. *J. Comput. Chem.* **1982**, *3*, 317−328. (e) Bader, R. F. W. *Acc. Chem. Res.* **1985**, *18*, 9−15. (f) Tang, T. H.; Bader, R. F. W.; MacDougall, P. J. *Inorg. Chem.* **1985**, *24*, 2047−2053. (g) Biegler-König, F.; Schönbohm, J.; Bayles, D. *J. Comput. Chem.* **2001**, *22*, 545−559. (h) Biegler-König, F.; Schönbohm, J. *J. Comput. Chem.* **2002**, *23*, 1489−1494.
(34) Molina, J.; Dobado, J. A. *Theor. Chem. Acc.* **2001**, *105*, 328−337.
(35) Dobado, J. A.; Martinez-Garcia, H.; Molina, J.; Sundberg, M. R. *J. Am. Chem. Soc.* **2000**, *122*, 1144−1149.
(36) Ignatov, S. K.; Rees, N. H.; Tyrrell, B. R.; Dubberley, S. R.; Razuvaev, A. G.; Mountford, P.; Nikonov, G. I. *Chem. - Eur. J.* **2004**, *10*, 4991−4999.
(37) Tripathi, S. K.; Patel, U.; Roy, D.; Sunoj, R. B.; Singh, H. B.; Wolmershäuser, G.; Butcher, R. J. *J. Org. Chem.* **2005**, *70*, 9237−9247.
(38) Boyd, R. J.; Choi, S. C. *Chem. Phys. Lett.* **1986**, *129*, 62−65.
(39) Carroll, M. T.; Bader, R. F. W. *Mol. Phys.* **1988**, *65*, 695−722.
(40) Grabowski, S. J. *J. Phys. Chem. A* **2001**, *105*, 10739−10746.
(41) (a) Espinosa, E.; Alkorta, I.; Elguero, J.; Molins, E. *J. Chem. Phys.* **2002**, *117*, 5529−5542. (b) Rozas, I.; Alkorta, I.; Elguero, J. *J. Am. Chem. Soc.* **2000**, *122*, 11154−11161. (c) Espinosa, E.; Molins, E.; Lecomte, C. *Chem. Phys. Lett.* **1998**, *285*, 170−173.
(42) Domagała, M.; Grabowski, S. J.; Urbaniak, K.; Mloston, G. *J. Phys. Chem. A* **2003**, *107*, 2730−2736.
(43) Grabowski, S. J.; Sokalski, W. A.; Leszczynski, J. *J. Phys. Chem. A* **2005**, *109*, 4331−4341.
(44) Domagala, M.; Grabowski, S. J. *J. Phys. Chem. A* **2005**, *109*, 5683−5688.
(45) Parthasarathi, R.; Subramanian, V.; Sathyamurthy, N. *J. Phys. Chem. A* **2006**, *110*, 3349−3351.
(46) Nakanishi, W.; Nakamoto, T.; Hayashi, S.; Sasamori, T.; Tokitoh, N. *Chem. - Eur. J.* **2007**, *13*, 255−268.
(47) (a) Nakanishi, W.; Hayashi, S.; Narahara, K. *J. Phys. Chem. A* **2009**, *113*, 10050−10057. (b) Nakanishi, W.; Hayashi, S.; Narahara, K. *J. Phys. Chem. A* **2008**, *112*, 13593−13599.
(48) Nakanishi, W.; Hayashi, S. *Curr. Org. Chem.* **2010**, *14*, 181−197.
(49) (a) Nakanishi, W.; Hayashi, S. *J. Phys. Chem. A* **2010**, *114*, 7423−7430. (b) Nakanishi, W.; Hayashi, S.; Matsuiwa, K.; Kitamoto, M. *Bull. Chem. Soc. Jpn.* **2012**, *85*, 1293−1305.
(50) Hayashi, S.; Matsuiwa, K.; Miza, H.; Nakanishi, W. *Heteroat. Chem.* **2014**, *25*, 449−472.
(51) Frisch, M. J.; et al. *Gaussian09, revision D.01*; Gaussian, Inc.: Wallingford, CT, 2009. A complete list of authors is given in the Supporting Information.
(52) For the 6-311G(3d) basis sets, see: (a) Binning, R. C., Jr.; Curtiss, L. A. *J. Comput. Chem.* **1990**, *11*, 1206−1216. (b) Curtiss, L. A.; McGrath, M. P.; Blaudeau, J.-P.; Davis, N. E.; Binning, R. C., Jr.; Radom, L. *J. Chem. Phys.* **1995**, *103*, 6104−6113. (c) McGrath, M. P.; Radom, L. *J. Chem. Phys.* **1991**, *94*, 511−516. (d) For the diffuse functions (+ and + +), see: Clark, T.; Chandrasekhar, J.; Spitznagel, G. W.; Schleyer, P. v. R. *J. Comput. Chem.* **1983**, *4*, 294−301.
(53) (a) For inner and valence shells: Koga, T.; Yamamoto, S.; Shimazaki, T.; Tatewaki, H. *Theor. Chem. Acc.* **2002**, *108*, 41−45. (b) For valence correlated set: Sekiya, M.; Noro, T.; Osanai, Y.; Koga, T. *Theor. Chem. Acc.* **2001**, *106*, 297−300.
(54) (a) Møller, C.; Plesset, M. S. *Phys. Rev.* **1934**, *46*, 618−622. (b) Gauss, J. *J. Chem. Phys.* **1993**, *99*, 3629−3643. (c) Gauss, J. *Ber. Bunsenges, Phys. Chem.* **1995**, *99*, 1001−1008.
(55) Zhao, Y.; Truhlar, D. G. *Theor. Chem. Acc.* **2008**, *120*, 215−241.
(56) Vydrov, O. A.; Scuseria, G. E. *J. Chem. Phys.* **2006**, *125*, 234109-1−234109-9.
(57) Yanai, T.; Tew, D. P.; Handy, N. C. *Chem. Phys. Lett.* **2004**, *393*, 51−57.
(58) Peach, M. J. G.; Benfield, P.; Helgaker, T.; Tozer, D. J. *J. Chem. Phys.* **2008**, *128*, 044118−1−044118−8.
(59) Becke, A. D. *J. Chem. Phys.* **1993**, *98*, 5648−5652.
(60) Lee, C.; Yang, W.; Parr, R. G. *Phys. Rev. B: Condens. Matter Mater. Phys.* **1988**, *37*, 785−789.
(61) Knowles, P. J.; Andrews, J. S.; Amos, R. D.; Handy, N. C.; Pople, J. A. *Chem. Phys. Lett.* **1991**, *186*, 130−136.
(62) The AIM2000 program (Version 2.0) is employed to analyze and visualize atoms-in-molecules: Biegler-König, F. *J. Comput. Chem.* **2000**, *21*, 1040−1048. See also ref 32a.
(63) For the $m \times n$ matrix representation, m corresponds to the number of atoms and n (=3) to the x, y, and z components of the space.
(64) The values of w = (0), ±0.1, and ±0.2 in $r = r_o + wa_o$ were employed for the perturbed structures in POM in refs 47 and 48, since the bond order (BO)[69] becomes $^2/_3$ and $^3/_2$ times larger at w = +0.2 and −0.2 relative to the original values at w = 0, respectively. However, it seems better to employ the perturbed structures as close as possible to the fully optimized ones in NIV in ref 49. The perturbed structures closer to the fullly optimized one will reduce the errors in the QTAIM functions with the perturbed structures generated by NIV and/or POM. Therefore, w = (0), ±0.05, and ±0.1 for $r = r_o + wa_o$ are employed for the analysis in this paper.
(65) It is achieved by changing the corresponding parameters in Gaussian 09 from the default values to print out the normal coordinates of five digits for the purpose.
(66) Nakanishi, W.; Hayashi, S. *J. Phys. Chem. A* **2013**, *117*, 1795−1803.
(67) A BCP will exist at the midpoint between E and E′ in E−E′, if E = E′. Where is BCP in E−E′, when E ≠ E′? BCP will be closer to E than to E′, where $\chi_E > \chi_{E'}$. The results are usually observed in QTAIM analysis, although the covalent radii of E′ must be larger than that of E. The bond path between E and E′ seems substantially straight along the E−E′ bond.
(68) In such cases, data are plotted inversely as $H_b(\mathbf{r}_c) - V_b(\mathbf{r}_c)/2$ versus $H_b(\mathbf{r}_c)$, although some modification in eq 5 is necessary to obtain the θ_p values.
(69) The bond order (BO), which corresponds to the strength of a chemical bond, is correlated to $\rho_b(\mathbf{r}_c)$ by the form shown below, where A and B are constants which depend on the nature of the bonded atoms.[32b] $BO = \exp[A\rho_b(\mathbf{r}_c) - B]$.

DOI: 10.1021/acs.joc.5b01794
J. Org. Chem. 2015, 80, 11963−11976